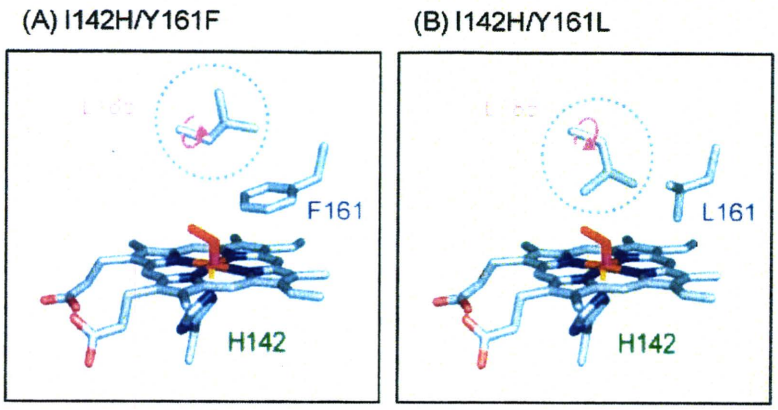

Fig. 5. Structural models of the heme pocket in dioxygenated rHSA(I142H/Y161F)-heme and rHSA(I142H/Y161L)-heme. Distal-side steric effect of Leu-185 on O_2 and CO association

(R-state). To develop this O_2 carrying albumin as a blood substitute, it is required to regulate O_2 binding affinity suitable for Hb, Mb, and human RBC. One approach to increasing O_2 binding affinity of rHSA(double mutant)-heme would be to introduce another histidine into an appropriate position on the distal side of the heme pocket. The N_ε atom of histidine may act as a proton donor to form an hydrogen bond with the coordinated O_2.

In Hb and Mb, His-64 on the distal side of the heme plays a crucial role for tuning their ligand affinity, as shown by a neutron diffraction study and high-resolution X-ray structureal analysis.[54,55] A number of systematic investigations on site-directed mutants of Hb and Mb show that the overall polarity and packing of the distal residues are key factors in regulating the equilibrium constants for ligand binding.[53,56,57] Then, we generated new rHSA(triple mutant)-heme complexes, in which the specific third mutation was introduced near the O_2 binding site. Another important point in this design is to prevent the formation of a six-coordinate low-spin ferrous complex. Bis-histidyl hemochromes are generally autoxidized by O_2.[58–60] Therefore, the distal amino acid must be located relatively far (>4 Å) from the central iron. Our simulation indicated that the favorable position for the distal His insertion was Leu-185 (**Fig. 2**). Thus the polarity of the distal side of the heme in rHSA(I142H/Y161F) and rHSA(I142H/Y161L) was increased by replacing Leu-185 with asparagines, glutamine, and histidine using site-directed mutagenesis. Five triple mutants [rHSA(I142H/Y161F/L185N), rHSA(I142H/Y161L/L185N), rHSA(I142H/Y161F/L185Q), rHSA(I142H/Y161L/L185Q), and rHSA(I142H/Y161F/L185H)] (**Fig. 2**) were thus cloned and their heme complexes were prepared.

The rHSA(I142H/Y161F/L185N)-heme, rHSA(I142H/Y161L/L185N)-heme, and rHSA(I142H/Y161L/L185Q)-heme showed a visible absorption band at 558–559 nm with a small shoulder at 530 nm, that was similar to the spectrum observed for the rHSA(I142H/Y161F)-heme, rHSA(I142H/Y161L)-heme, deoxy Mb[47] and synthetic chelated-heme.[48] The spectral patterns indicated the formation of a five-*N*-coordinate high-spin complex. In the spectra of the rHSA(I142H/Y161F/L185Q)-heme and rHSA(I142H/Y161F/L185H)-heme, the β band at 528 nm appeared slightly sharp, suggesting partial formation of a six-*N*-coordinate heme complex. On the basis of all the UV-vis absorption and MCD spectral results, we concluded that the heme is axially coordinated by His-142 in rHSA(triple mutant) and forms a five-*N*-coordinate high-spin ferrous complex under an Ar atmosphere in the case of I142H/Y161F/L185N, I142H/Y161L/L185N, and I142H/Y161L/L185Q mutants (**Fig. 6A, B, D**). In addition to the His-142 ligation, Gln-185 and His-185 partially interact with the sixth coordinate position of the central Fe^{2+} ion of the heme in I142H/Y161F/L185Q and I142H/Y161F/L185H mutants in spite of the bulky Phe-161 (**Fig. 6C, E**). We suppose that the rHSA (I142H/Y161L/L185Q)-heme may also produce a six-coordinate low-spin complex, because the small Leu-161 allows free rotation of Gln-185. However, it gave a five-coordinate high-spin ferrous complex. This suggests that the long Gln-185 may interact with neighboring amino acids (**Fig. 6D**).

With exposure of the rHSA(I142H/Y161F/L185N)-heme and rHSA(I142H/Y161L/L185N)-heme solutions to O_2, the UV-vis absorptions changed to that of the O_2 adduct complex at 22°C. However, the rHSA(I142H/Y161L/L185Q)-heme complex bound O_2 only at 5°C and was oxidized at 22°C. This rapid oxidation may suggest that the distal side of the heme has an open structure, which allows easy access of water to the heme. The rHSA(I142H/Y161F/L185Q)-heme and rHSA(I142H/Y161F/L185H)-heme complexes could not bind O_2 even at low temperature. After introducing CO gas, all hemoproteins produced stable carbonyl complexes with identical absorption spectral patterns.[47,48]

In rHSA(double mutant)-heme complexes, there exists

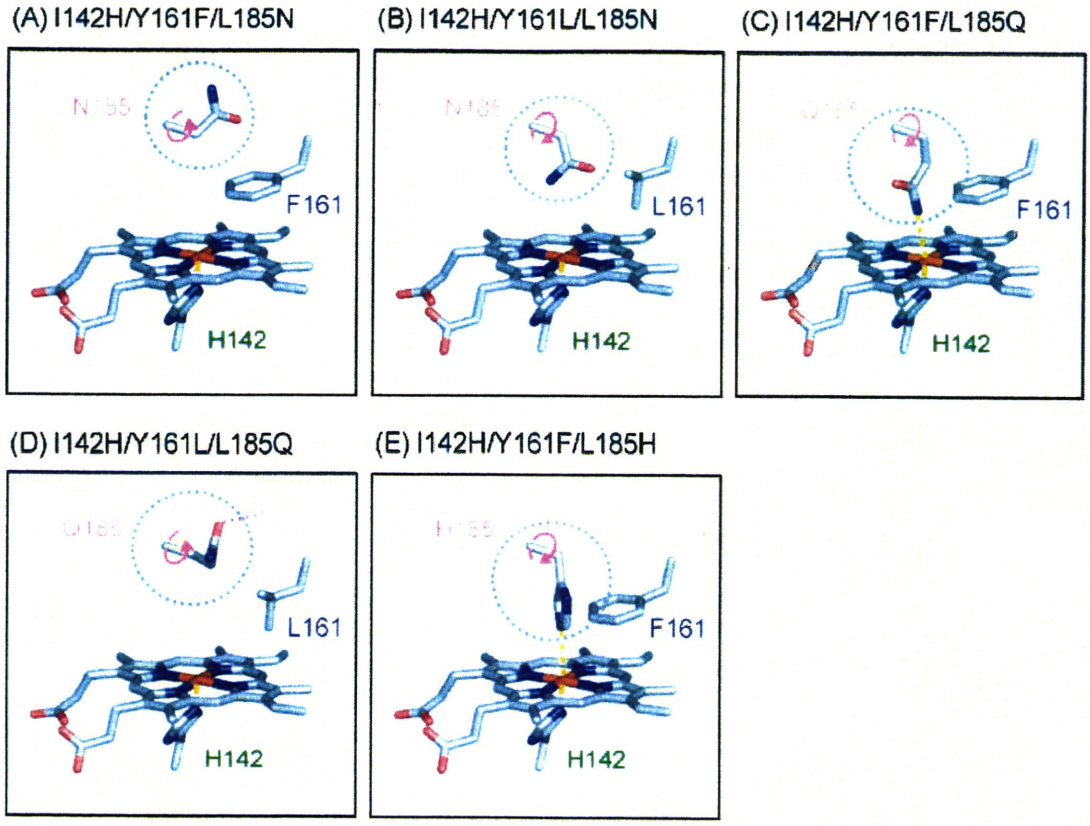

Fig. 6. Structural models of the heme pocket in rHSA(triple mutant)-heme complexes
Distal-side effect of engineered amino acid at position 185.

two geometries of axial His-142 coordination to the central Fe^{2+} ion of the heme (species I and II). In species I, the proximal His coordinates to the heme without strain, while in species II, the His-Fe ligation involves some distortion, resulting in weaker O_2 binding. In rHSA(triple mutant)-hemes, this alternative geometry of the heme plane would also arise in the same manner. As expected, the binding behavior of O_2 for rHSA(I142H/Y161F/L185N)-heme and rHSA(I142H/Y161L/L185N)-heme was almost the same as that of the original double mutants.

The k_{off}^{CO} is normally an indicator of bending strain in the proximal His coordination to the central Fe^{2+} ion.[49,50] The rHSA(I142H/Y161F)-heme, rHSA(I142H/Y161L)-heme, rHSA(I142H/Y161F/L185N)-heme, and rHSA(I142H/Y161L/L185N)-heme exhibited similar k_{off}^{CO} in species I (0.008–0.013 s^{-1}) which were identical to that of Hbα (R-state) (0.009 s^{-1}) (**Table 2**).[61] This indicates that the axial His-142 ligation to the heme in these artificial hemoproteins has the same features as that of Hb.

O_2 and CO binding parameters for the rHSA (I142H/Y161F)-heme and rHSA(I142H/Y161F/L185N)-heme complexes did not show any significant differences. The bulky benzyl side-chain of Phe-161 may retard rotation of the polar amide group of Asn-185 (**Fig. 6A**). In contrast, there are significant differences in the O_2 and CO binding parameters for rHSA(I142H/Y161L)-heme and rHSA(I142H/Y161L/L185N)-heme. The Asn-185 induced 18-fold and 10-fold increases in the O_2 binding affinity for species I and II. The increase was mainly due to the 6–11-fold reduction of $k_{off}^{O_2}$. It is noteworthy that the high O_2 binding affinity ($P_{1/2}^{O_2}$: 1 Torr) for rHSA (I142H/Y161L/L185N)-heme is close to that of natural Hbα (0.24 Torr)[51,52] and Mb (0.5 Torr)[53] (**Table 2**).

Further tuning of O_2 binding affinity of rHSA(triple mutant)-heme complexes: The O_2 binding equilibrium and kinetics of rHSA-heme complexes are significantly enhanced by site-directed mutagenesis. However, for artificial rHSA-heme solutions to provide effective O_2 transport from lungs to tissues in the body, the O_2 binding affinity of HSA(I142H/Y161L/L185N)-heme should be reduced to that of human RBC ($P_{1/2}^{O_2}$: 8 Torr).[62] This requires an O_2 binding affinity intermediate between the values for rHSA(I142H/Y161L)-heme and rHSA(I142H/Y161L/L185N)-heme.

We thus designed new triple mutants, rHSA(I142H/Y161L/R186L) and rHSA(I142H/Y161L/R186F) (**Fig. 2**). An important structural factor in these mutants is Y161L, which allows rotation of the isopropyl group of Leu-185 above the O_2 coordination site. The reduced ferrous forms produced the five-*N*-coordinate high-spin

complexes under an Ar atmosphere and formed the O_2 adduct complex after bubbling O_2 gas. The distinct features of all the spectra were similar to those of the rHSA(I142H/Y161L)-heme.

Following laser flash photolysis, the absorption decay associated with O_2 recombination to the rHSA(I142H/Y161L/R186L)-heme and rHSA(I142H/Y161L/R186F)-heme was monophasic. The kinetics for CO rebinding were still composed of two single-exponentials, consistent with the existence of two different geometries of the axial His-142 coordination to the central Fe^{2+} ion of the heme.

The rHSA(I142H/Y161F)-heme binds O_2 with higher affinity than rHSA(I142H/Y161L) because of the presence of Leu at position 161, which allows a downward rotation of the L185 side chain and reduces the affinity. However, insertion of Leu or Phe at position 186 in the presence of Leu-161 yielded $k_{on}^{O_2}$ and k_{on}^{CO} 3–4-fold higher than those of rHSA(I142H/Y161L)-heme. The presence of a hydrophobic residue at position 186 may restrict the downward rotation of the isopropyl group of Leu-185 (**Fig. 7**). Overall, the O_2 and CO binding parameters of rHSA(I142H/Y161L/R186L)-heme and rHSA(I142H/Y161L/R186F)-heme were more similar to those of rHSA(I142H/Y161F)-heme, but their O_2 dissociation rate constants were 3–4-fold higher than found for rHSA(I142H/Y161F)-heme, which modestly reduced O_2 binding affinity. This may be due to increase in hydrophobicity in the distal pocket. It is noteworthy that O_2 binding affinity of the rHSA(I142H/Y161L/R186L)-heme ($P_{1/2}^{O_2}$: 10 Torr) and rHSA(I142H/Y161L/R186F)-heme ($P_{1/2}^{O_2}$: 9 Torr) is essentially the same to that of human RBC ($P_{1/2}^{O_2}$: 8 Torr).

Circulation life of rHSA complexes: It would be of great importance to study the in vivo circulation behavior of rHSA(mutant)-heme complex for practical medical applications. This investigation is currently undergoing, but we have several results on the HSA-FeP complex. In general, the ligand molecule complexed with HSA gradually dissociates from the protein when infused into the body, since the ligand is noncovalently bound into the hydrophobic cavity of HSA. We found that surface modification of HSA-FeP by poly(ethylene glycol) (PEG) significantly improved the circulation lifetime of FeP in animals and thereby retained its O_2-transporting ability for a long period.[34] Interestingly, the linkage form of the PEG chain dramatically affects the circulation persistence of FeP. Maleimide-PEG conjugates showed 6–8-fold longer lifetime compared to the succinimide-PEG analogue.[34] PEG modified rHSA(mutant)-heme would also remain in the circulatory system with long persistence, which could be a potential advantage for O_2 delivery to the tissues.

HSA Incorporating C_{60} Fullerene as Photosensitizer for Photodybamic Therapy

Structure and photophysical properties of HSA-fullerene complex: Photodynamic therapy (PDT) is advanced cancer treatment involving a photosensitizer, visible light and tissue O_2.[64,65] Singlet oxygen ($^1O_2$) formed by energy transfer from photoexcited state of sensitizer is highly cytotoxic and has been implicated as an intermediary species leading to cell death in tumors. To accelerate this $^1O_2$ formation, various organic dyes, especially porphyrin derivatives, have been designed as photosensitizers.[66] The most widely used reagent in clinical PDT is Photofrin, which is a mixture of water soluble hematoporphyrin oligomers.[63,64,69] Several porphyrin or chlorin compounds are also being tested.[63,64,68,69] Another potential regent is 5-aminolevulinic acid (ALA).[70,71] ALA enters into cancer cells and induces the biosynthesis of protoporphyrin IX (PP). Buckminster[60]fullerene (C_{60}) produces $^1O_2$ by energy transfer with extremely high quantum yield (Φ_Δ: 0.96, $\lambda_{exc} = 532$ nm)[72,73] and shows strong resistance against laser irradiation. Consequently, various water-soluble fullerenes and fullerene-polymer hybrids have been synthesized as new photosensitizing reagents.[73–76] However, to evaluate the biological function of fullerene, one must investigate the structure and properties of the HSA-fullerene complex, because exogenous compounds administered into the bloodstream are generally captured by HSA. We prepared HSA complexed with a tris(dicarboxymethylene)[60] fullerene C_3-isomer (HSA-CF) and characterized its photoinduced energy transfer to O_2 to produce $^1O_2$ and its cytotoxicity to cancer cells under visible light.[43]

The HSA-CF complex was prepared essentially as described previously for HSA-hemin complex.[41] The gel permeation chromatogram of the orange-colored protein exhibited a single elution peak. This indicates that CF efficiently binds to HSA. The UV-vis absorption spectroscopic features of the HSA-CF solution are the sum of those from the individual HSA and CF (**Fig. 8**), which implies that CF is monomolecularly incorporated into HSA and no specific interaction occurs between the two molecules at the ground state. Gozin *et al.* reported that CF is incorporated into the subdomain IIA of HSA with a binding constant of $1.2 \times 10^7\ M^{-1}$ by fluorescent quenching experiments.[77]

The HSA-CF complex was sufficiently stable to apply to HPLC measurement. In the elution profile, only a single peak was observable. The ratio of peak intensity monitored at 280 nm (based on HSA) and at 490 nm (based on CF) ($I_{280}/I_{490} = 30$) was exactly the same as the absorbance ratio at 280 nm and 490 nm in the UV-vis absorption spectrum (A_{280}/A_{490}) of HSA-CF, which suggests that all CF molecules are eluted within the HSA fraction. The ESI-TOF mass spectroscopy showed a distinct ion

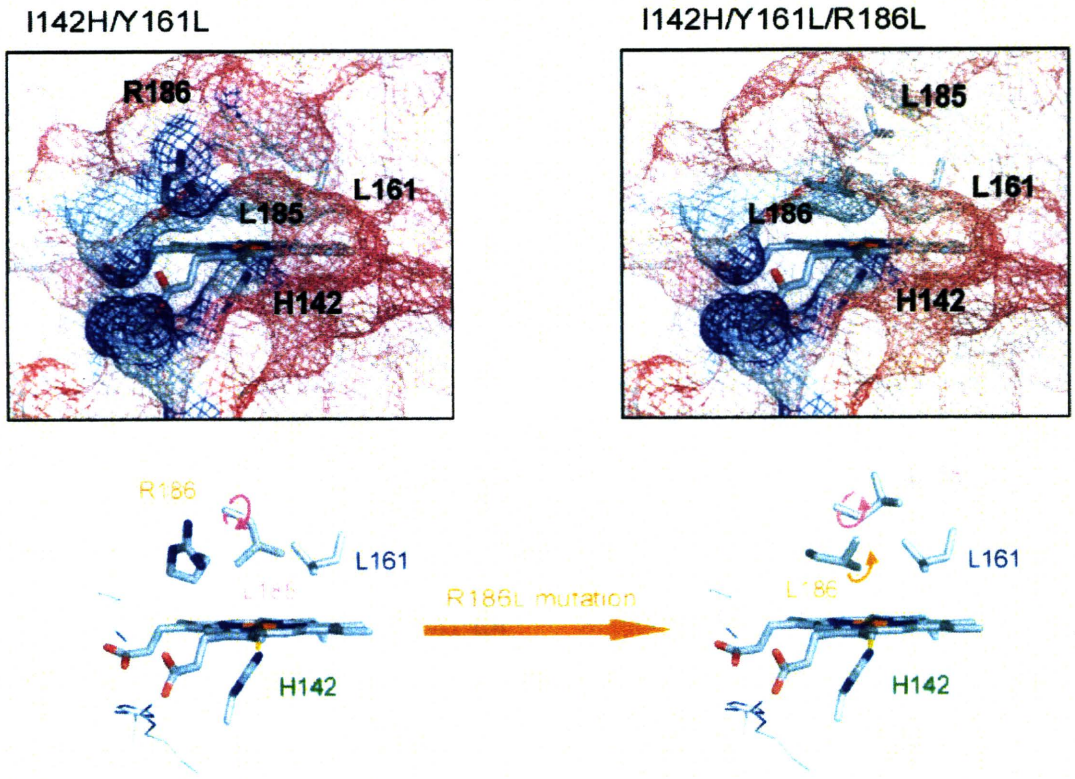

Fig. 7. Structural models of rHSA(I142H/Y161L)-heme and rHSA(I142H/Y161L/R186L)-heme complexes
Introduction of R186L mutation may induce upward rotation of the L185 residue.

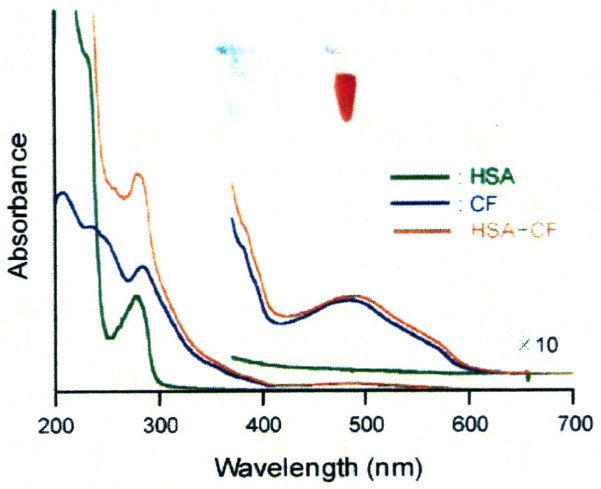

Fig. 8. UV-vis absorption spectrum of HSA-CF, CF, and HSA in 50 mM phosphate buffered solution (pH 7.0)
Inset photographs are 5 g dL^{-1} HSA (left) and HSA-CF (right) solutions.

peak at 67,587 Da, which corresponds to the mass of the equivalent complex of HSA-CF. CD spectral patterns and intensities of HSA-CF were identical to those of HSA. We inferred that fullerene binding did not change the highly ordered structure of the protein. The incorporation of negatively charged CF may influence the surface charge distribution of albumin. However, isoelectric focusing of HSA-CF indicated the same isoelectric point with HSA.

We used small-angle X-ray scattering (SAXS) to evaluate the globular particle structure and protein-protein interactions of HSA-CF. The pair-distance distribution functions [$p(r)$] of HSA-CF and HSA were almost identical to the curve calculated from crystallographic data of HSA (**Fig. 9A**). This demonstrates that the maximum diameter (D_{max}: *ca.* 8 nm) and three-dimensional particle shape of HSA are not changed by complexation of the CF moelcule. The extrapolated structure factors [$S(q\rightarrow 0)$] reflect the net repulsive forces between the protein molecules. Plots of $S(q\rightarrow 0)$ for HSA-CF and HSA were lower than that predicted for hardsphere with an identical volume fraction (**Fig. 9B**), this being due to the strong electrostatic repulsion between the proteins. The perfectly same lines of HSA-CF and HSA suggest that the HSA molecule preserves its surface net charge upon CF binding. We conclude that CF is accommodated into the deep hydrophobic cavity of HSA with internal charge neutralization, and it does not induce marked change in the globular particle size or surface charge distribution of HSA.

Photoexcited triplet state of the HSA-CF complex and $^1O_2$ production: Photoexcitation of fullerenes generates the singlet state, which undergoes intersystem crossing to the triplet state in high yield.[72,73] Laser

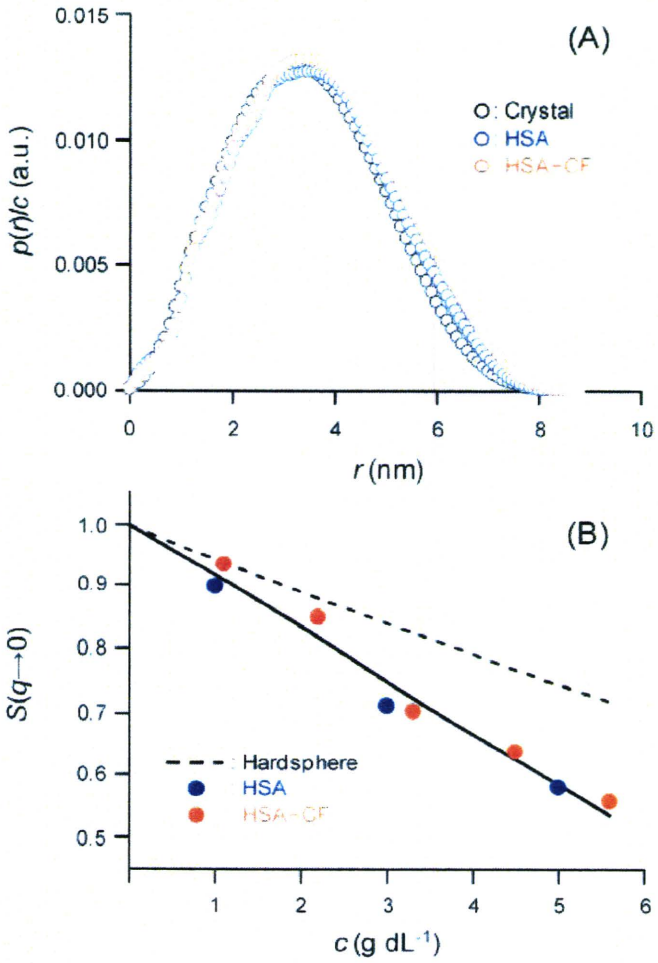

Fig. 9. (A) Pair-distance distribution functions [$p(r)$] obtained from SAXS measurements of HSA-CF and HSA in 150 mM PBS solutions. (B) The extrapolated structure factors [$S(q\rightarrow 0)$] of HSA-CF and HSA

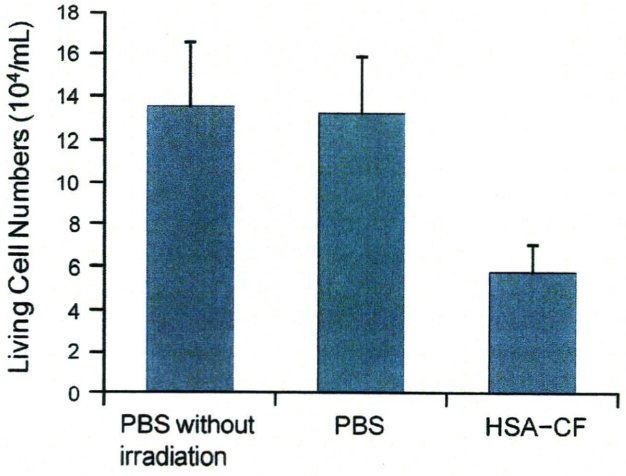

Fig. 10. Living cell numbers of LY80 with HSA-CF and PBS after visible light irradiation (20 mW cm^{-2}, 2 h, 36 ± 1°C)
Each value represents the mean ± SD ($n = 4$).

flash photolysis of the HSA-CF solution under an N_2 atmosphere gave a triplet-triplet (T-T) absorption spectrum of the $^3CF^*$ chromophore ($\lambda_{max} = 740$ nm).[73,75,78] The time course of the absorbance decay was composed of a single exponential kinetics with a lifetime (τ_T) of 46 μs. In the presence of O_2, the triplet lifetime of HSA-CF markedly decreased. Energy transfer took place from HSA-$^3CF^*$ to the O_2 molecule to generate active $^1O_2$. The Stern-Volmer plot depicts a linear correlation for O_2 concentrations (0–1.0 mM), giving the quenching rate constant [$k_q(O_2)$: 2.2×10^8 $M^{-1}s^{-1}$]. The intensity of the visible band of HSA-CF ($\lambda_{max} = 490$ nm) did not change after 10^3-times laser flash irradiation ($\lambda_{ex} = 532$ nm, 0.5 W) under air. In contrast, Soret band of HSA-PP was 6% bleached after identical flash photolysis. The light resistance of CF chromosphere is significantly higher than that of PP.

The quantum yield of $^1O_2$ production (Φ_Δ) for HSA-CF was determined from the value of emission intensity of the $^1O_2$ (λ_{max} 1270 nm).[79] Φ_Δ of HSA-CF (0.46) was in the same range as that of monomeric CF (0.48), methylene blue (0.52), protoporphyrin IX dimethyl ester in benzene (0.59),[79] and substituted fullerenes in organic solvent,[80,81] but somewhat lower than for rose bengal (0.75), hematoporphyrin in methanol (0.74),[82] and pristine C_{60} (0.96) in benzene.[72] Substitution of the C_{60} fullerene causes perturbation of the electronic structure of the fullerene core, thereby decreasing the quantum yield for $^1O_2$ formation.[80,81]

Cytotoxicity of HSA-CF complex: The cytotoxicity and photodynamic activity of the HSA-CF complex to LY80 tumor cells was evaluated. The cell cultures were first incubated for 24 h in the dark with HSA-CF (20 μM) at 37°C under 5% CO_2. Cell numbers after incubation were identical to those of the control group with the phosphate buffered saline (PBS, pH 7.4) solution. The HSA-CF complex showed no dark cytotoxicity. The cell culture plate was then exposed to visible light of 350–600 nm (20 mW cm^{-2}) for 2 h at 36 ± 1°C. Some cells mixed with HSA-CF showed morphological change after light irradiation, whereas the PBS group did not show any morphological change of the cells. The living cell numbers of the PBS groups with and without light were almost the same (**Fig. 10**), which means that light exposure did not affect the LY80 tumor cells in this experimental condition. The living cell numbers of the HSA-CF group were lower than that of the PBS group; 57% cell death occurred by visible light irradiation. This clearly implies that the HSA-CF complex acts as a photosensitizer for PDT.

Conclusions

Transport of O_2 by the rHSA(mutant)-heme complex may be of great medical importance not only as a blood alternative, but also as an O_2-therapeutic fluid. The first generation of rHSA(double mutant)-heme complexes can

be successfully engineered to bind to O_2. However, these complexes did not show optimal O_2 binding affinity. We attempted to modify the heme pocket architecture to refine O_2 binding properties. By focusing on modification on the distal side of the heme pocket, we prepared rHSA(triple mutant)-heme complexes with a broad range of O_2 binding affinity. The highest affinity mutant rHSA(I142H/Y161L/L185N) contains Asn-185, which has a short amide side-chain that enhances O_2 binding affinity. In a different approach, substitution of the polar Arg-186 with Leu or Phe caused useful reduction in O_2 binding affinity, yielding $P_{1/2}^{O_2}$ almost identical to that of human RBC.

Amphiphilic C_{60} fullerene also be adopted as functional ligand for HSA. The HSA-CF complex is easily excited by visible light and shows a high charge transfer rate constant for O_2. The efficiency of $^1O_2$ production of this artificial protein is in the same range as common dyes. The HSA-CF complex does not have dark cytotoxicity, but engenders cell death under visible light irradiation.

In both the HSA-based O_2 carrier and photosensitizer, the protein plays a crucial role for solubilizing the heme and CF in aqueous medium up to ca. 3 mM. Even at high concentration, shielding of the chromophore by negatively charged HSA inhibits oxidation of the dioxygenated heme via μ-oxo dimer formation and a bimolecular Triplet-Triplet annihilation of excited $^3CF^*$. Furthermore, in the case of the rHSA-heme complex, a pair of site-specific mutations is essential to confer O_2 binding capability on the heme. In contrast, no mutation is required for photosensitizing HSA-CF; replacement of some amino acid around the CF binding site may enhance the photophysical properties of the CF molecule. rHSA is now manufactured on an industrial scale using yeast species *Pichia pastoris*,[83] which allows these functional proteins for use in practical applications.

Acknowledgments: This work was supported by PRESTO "Control of Structure and Functions", JST, Grant-in-Aid for Scientific Research (No. 20350058) from JSPS, and Health Science Research Grants (Regulatory Science) from MHLW Japan. The authors thank to Prof. Dr. Eishun Tsuchida for his precious suggestions and Prof. Dr. Stephen Curry (Imperial College London) for his valuable comments and cooperation on protein structure and site-directed mutagenesis. Prof. Koichi Kobayashi and Prof. Hirohisa Horinouchi (Keio University) are also gratefully acknowledged for their supports on animal experiments. We are grateful to Dr. Takaaki Sato for his skillful experiments and evaluation on SAXS measurements. X.Q. thanks a JSPS Postdoctoral Fellowship for Foreign Researchers.

References

1) Peters, T.: All about Albumin: Biochemistry, Genetics and Medical Applications. San Diego, Academic Press, 1996.
2) Kragh-Hansen, U.: Molecular sepcts of ligand binding to serum albumin. *Pharmacol. Rev.*, **33**: 17–53 (1981).
3) Kragh-Hansen, U.: Structure and ligand-binding properties of human serum-albumin. *Danish Med. Bull.*, **37**: 57–84 (1990).
4) Curry, S., Madelkow, H., Brick, P. and Franks, N.: Crystal structure of human serum albumin complexed with fatty acid reveals an asymmetric distribution of binding sites. *Nat. Struct. Biol.*, **5**: 827–835 (1998).
5) Curry, S., Brick, P. and Franks, N.: Fatty acid binding to human serum albumin: new insights from crystallographic studies. *Biochim. Biophys. Acta*, **1441**: 131–140 (1999).
6) Petitpas, I., Petersen, C. E., Ha, C.-E., Bhattacharya, A. A., Zunszain, P. A., Ghuman, J., Bhagavan, N. V. and Curry, S.: Structural basis of albumin-thyroxine interactions and familial dysalbuminemic hyperthyroxinemia. *Proc. Natl. Acad. Sci. USA*, **100**: 6440–6445 (2003).
7) Zunszain, P. A., Ghuman, J., McDonagh, A. F. and Curry, S.: Crystallographic analysis of human serum albumin complexed with 4*Z*,15*E*-birirubin-IXα. *J. Mol. Biol.*, **381**: 394–406 (2008).
8) Ghuman, J., Zunszain, P. A., Petotpas, I., Bhattacharya, A. A., Otagiri, M. and Curry, S.: Structural basis of the drug-binding specificity of human serum albumin. *J. Mol. Biol.*, **353**: 38–52 (2005).
9) Fairley, N. H.: Methemalbumin (pseudo-methemoglobin). *Nature*, **142**: 1156–1157 (1938).
10) Muller-Eberhard, U. and Morgan, W. T.: Porphyrin-binding proteins in serum. *Ann. N.Y. Acad. Sci.*, **244**: 624–650 (1975).
11) Adams, P. A. and Berman, M. C.: Kinetics and mechanism of the interaction between human serum albumin and monomeric haemin. *Biochem. J.*, **191**: 95–102 (1980).
12) He, X. M. and Carter, D. C.: Atomic structure and chemistry of human serum albumin, *Nature*, **358**: 209–215 (1992).
13) Carter, D. C. and Ho, J. X.: Structure of serum albumin. *Adv. Protein Chem.*, **45**: 153–203 (1994).
14) Wardell, M., Wang, Z., Ho, J. X., Robert, J., Ruker, F., Rubel, J. and Carter, D. C.: The atomic structure of human serum methemalbumin at 1.9 Å. *Biochem. Biophys. Res. Commun.*, **291**: 813–819 (2002).
15) Zunszain, P. A., Ghuman, J., Komatsu, T., Tsuchida, E. and Curry, S.: Crystal structural analysis of human serum albumin complexed with hemin and fatty acid. *BMC Struct. Biol.*, **3**: 6 (2003).
16) Monzani, E., Bonafè, B., Fallarini, A., Redaelli, C., Casella, L., Minchiotti, L. and Galliano, M.: Enzymatic properties of human serum albumin. *Biochim. Biophys. Acta*, **1547**: 302–312 (2001).
17) Mahammed, A. and Gross, Z.: Albumin-conjugated corrole metal complexes: extremely simple yet very efficient biomimetic oxidation Systems. *J. Am. Chem. Soc.*, **127**: 2883–2887 (2005).
18) Reetz, M. T. and Jiao, N.: Copper-phthalocyanine conjugates of serum albumins as enantioselective catalysts in Diels-Alder reactions. *Angew. Chem. Int. Ed.*, **45**: 2416–2419 (2006).
19) Belgorodsky, B., Fadeev, L., Kolsenik, J. and Gozin, M.: Formation of a soluble state complex between pristine C_{60}-fullerene and native blood protein. *Chem. Bio. Chem.*, **7**: 1783–1789 (2006).
20) Komatsu, T., Hamamatsu, K., Wu, J. and Tsuchida, E.: Physicochemical properties and O_2-coordination structure of human serum albumin incorporating tetrakis(*o*-pivalamido) phenylpor-

phinatoiron(II) derivatives. *Bioconjugate Chem.*, **10**: 82–86 (1999).

21) Tsuchida, E., Komatsu, T., Mastukawa, Y., Hamamatsu, K. and Wu, J.: Human serum albumin incorporating tetrakis(*o*-pivalamido)phenylporphinatoiron (II) derivative as a totally synthetic O_2-carrying hemoprotein. *Bioconjugate Chem.*, **10**: 797–802 (1999).

22) Komatsu, T., Hamamatsu, K. and Tsuchida, E.: Cross-linked human serum albumin dimer incorporating sixteen (tetraphenylporphinato)iron(II) derivatives: synthesis, characterization, and O_2-binding property. *Macromolecules*, **32**, 8388–8391 (1999).

23) Tsuchida, E., Komatsu, T., Hamamatsu, K., Matsukawa, Y., Tajima, A., Yoshizu, A., Izumi, Y. and Kobayashi, K.: Exchange transfusion of albumin-heme as an artificial O_2-infusion into anesthetized rats: physiological responses, O_2-delivery and reduction of the oxidized hemin sites by red blood cells. *Bioconjugate Chem.*, **11**: 46–50 (2000).

24) Komatsu, T., Matsukawa, Y. and Tsuchida, E.: Kinetics of CO and O_2 binding to human serum albumin-heme hybrid. *Bioconjugate Chem.*, **11**: 772–776 (2000).

25) Komatsu, T., Matsukawa, Y. and Tsuchida, E.: Reaction of nitric oxide with synthetic hemoprotein, human serum albumin incorporating tetraphenylporphinatoiron(II) derivatives. *Bioconjugate Chem.*, **12**: 71–75 (2001).

26) Komatsu, T., Okada, T., Moritake, M. and Tsuchida, E.: O_2-binding properties of double-sided porphinatoiron(II)s with polar substituents and their human serum albumin hybrids. *Bull. Chem. Soc. Jpn.*, **74**: 1695–1702 (2001).

27) Komatsu, T., Matsukawa, Y. and Tsuchida, E.: Effect of heme structure on O_2-binding properties of human serum albumin-heme hybrids: intramolecular histidine coordination provides a stable O_2-adduct complex. *Bioconjugate Chem.*, **13**: 397–402 (2002).

28) Kobayashi, K., Komatsu, T., Iwamaru, A., Matsukawa, Y., Watanabe, M., Horinouchi, H. and Tsuchida, E.: Oxygenation of hypoxia region in solid tumor by administration of human serum albumin incorporating synthetic hemes. *J. Biomed. Mater. Res.*, **64A**: 48–51 (2003).

29) Tsuchida, E., Komatsu, T., Matsukawa, Y., Nakagawa, Y., Sakai, H., Kobayashi, K. and Suematsu, M.: Human serum albumin incorporating synthetic heme: red blood cell substitute without hypertension by nitric oxide scavenging. *J. Biomed. Mater. Res.*, **64A**: 257–261 (2003).

30) Komatsu, T., Oguro, Y., Teramura, Y., Takeoka, S., Okai, J., Anraku, M., Otagiri, M. and Tsuchida, E.: Physicochemical characterization of cross-linked human serum albumin dimer and its synthetic heme hybrid as an oxygen carrier. *Biochim. Biophys. Acta*, **1675**: 21–31 (2004).

31) Komatsu, T., Yamamoto, H., Huang, Y., Horinouchi, H., Kobayashi, K. and Tsuchida, E.: Exchange transfusion with synthetic oxygen-carrying plasma protein "albumin-heme" into an acute anemia rat model after seventy-percent hemodilution. *J. Biomed. Mater. Res.*, **71A**: 644–651 (2004).

32) Komatsu, T., Oguro, Y., Nakagawa, A. and Tsuchida, E.: Albumin clusters: structurally defined protein tetramer and oxygen carrier including thirty-two iron(II) porphyrins. *Biomacromolecules*, **6**: 3397–3403 (2005).

33) Nakagawa, A., Komatsu, T., Iizuka, M. and Tsuchida, E.: Human serum albumin hybrid incorporating tailed porphyrinatoiron(II) in the $\alpha,\alpha,\alpha,\beta$-conformer as an O_2-binding site. *Bioconjugate Chem.*, **17**: 146–151 (2006).

34) Huang, Y., Komatsu, T., Wang, R.-M., Nakagawa, A. and Tsuchida, E.: "Poly(ethylene glycol)-conjugated human serum albumin including iron porphyrins: surface modification improves the O_2-transporting ability. *Bioconjugate Chem.*, **17**: 393–398 (2006).

35) Huang, Y., Komatsu, T., Yamamoto, H., Horinouchi, H., Kobayashi, K. and Tsuchida, E.: PEGylated albumin-heme as an oxygen-carrying plasma expander: exchange transfusion into acute anemia rat model. *Biomaterials*, **27**: 4477–4483 (2006).

36) Komatsu, T., Huang, Y., Wakamoto, S., Abe, H., Fujihara, M., Azuma, H., Ikeda, H., Yamamoto, H., Horinouchi, H., Kobayashi, K. and Tsuchida, E.: Influence of O_2-carrying plasma hemoprotein "albumin-heme" on complement system and platelet activation in vitro and physiological responses to exchange transfusion. *J. Biomed. Mater. Res.*, **81A**: 821–826 (2007).

37) Nakagawa, A., Komatsu, T., Huang, Y., Lu, G. and Tsuchida, E.: O_2-binding albumin thin films: solid membranes of poly(ethylene glycol)-conjugated human serum albumin incorporating iron porphyrin. *Bioconjugate Chem.*, **18**: 1673–1677 (2007).

38) Nakagawa, A., Komatsu, T., Iizuka, M. and Tsuchida, E.: O_2 binding to human serum albumin incorporating iron porphyrin with a covalently linked methyl-L-histidine isomer. *Bioconjugate Chem.*, **19**: 581–584 (2008).

39) Horinouchi, H., Yamamoto, H., Komatsu, T., Huang, Y., Tsuchida, E. and Kobayashi, K.: Enhanced radiation response of a solid tumor with the artificial oxygen carrier 'albumin-heme', *Cancer Sci.*, **99**: 1274–1278 (2008).

40) Komatsu, T., Ohmichi, N., Zunszain, P. A., Curry, S. and Tsuchida, E.: Dioxygenation of human serum albumin having a prosthetic heme group in a tailor-made heme pocket. *J. Am. Chem. Soc.*, **126**: 14304–14305 (2004).

41) Komatsu, T., Ohmichi, N., Nakagawa, A., Zunszain, P. A., Curry, S. and Tsuchida, E.: O_2 and CO binding properties of artificial hemoproteins formed by complexing iron protoporphyrin IX with human serum albumin mutants. *J. Am. Chem. Soc.*, **127**: 15933–15942 (2005).

42) Komatsu, T., Nakagawa, A., Zunszain, P. A., Curry, S. and Tsuchida, E.: Genetic engineering of the heme pocket in human serum albumin: modulation of O_2 binding of iron protoporphyrin IX by variation of distal amino acids. *J. Am. Chem. Soc.*, **129**: 11286–11295 (2007).

43) Qu, X., Komatsu, T., Sato, T., Glatter, O., Horinouchi, H., Kobayashi, K. and Tsuchida, E.: Structure, photophysical property, and cytotoxicity of human serum albumin complexed with tris(dicarboxymethylene)[60]fullerene. *Bioconjugate Chem.*, **19**: 1556–1560 (2008).

44) Adachi, S., Nagano, S., Ishimori, K., Watanabe, Y., Morishima, I., Egawa, T., Kitagawa, T. and Makino, R.: Roles of proximal ligand in heme proteins: replacement of proximal hitidine of human myoglobin with cycteine and thyrosine by site-directed mutagenesis as models for P-450, chloroperoxidase, and catalase. *Biochemistry*, **32**: 241–252 (1991).

45) Hildebrand, D. P., Burk, D. L., Ferrer, J. C., Brayer, G. D. and Mauk, A. G.: The proximal ligand variant His93Tyr of horse heart myoglobin. *Biochemistry*, **34**: 1997–2005 (1995).

46) Nicoletti, F. P., Howes, B. D., Fittipaldi, M., Fanali, G., Fasano,

M., Ascenzi, P. and Smulevich, G.: Ibprofen induces an allosteric conformational transition in the heme complex of human serum albumin with siginificant effects on heme ligation. *J. Am. Chem. Soc.*, **130**: 11677–11688 (2008).

47) Antonini, E. and Brunori, M.: Hemoglobin and Myoglobin in Their Reactions with Ligands. Amsterdam, North-Holland Pub., 1971, pp 18.

48) Traylor, T. G., Chang, C. K., Geibel, J., Berzinis, A., Mincey, T. and Cannon, J.: Synthesis and NMR characterization of chelated heme models of hemoproteins. *J. Am. Chem. Soc.*, **101**: 6716–6731 (1979).

49) Collman, J. P., Brauman, J. I., Iverson, B. L., Sessler, J. L., Moris, R. M. and Gibson, Q. H.: O_2 and CO binding to iron(II) porphyrins: A comparison of the "picket fence" and "pocket" porphyrins. *J. Am. Chem. Soc.*, **105**: 3052–3064 (1983).

50) Traylor, T. G., Tsuchiya, S., Campbell, D., Mitchel, M., Stynes, D. and Koga, N.: Anthracene heme cyclophanes. Sterice in CO, O_2 and RNC Binding. *J. Am. Chem. Soc.*, **107**: 604–614 (1985).

51) Gibson, Q. H.: The reaction of oxygen with hemoglobin and the kinetic basis of the effect of salt on binding of oxygen. *J. Biol. Chem.*, **245**: 3285–3288 (1970).

52) Olson, J. S., Andersen, M. E. and Gibson, Q. H.: The dissociation of the first oxygen molecule from some mammalian oxyhemoglobins. *J. Biol. Chem.*, **246**: 5919–5923 (1971).

53) Rohlfs, R., Mathews, A. J., Carver, T. E., Olson, J. S., Springer, B. A., Egeberg, K. D. and Sliger, S. G.: The effects of amino acid substitution at position E7 (residue 64) on the kinetics of ligand binding to serum whale myoglobin. *J. Biol. Chem.*, **265**: 3168–3176 (1990).

54) Phillips, S. E. V. and Schoenborn, B. P.: Neuteon diffraction reveals oxygen-histidine hydrogen bond in oxymyoglobin. *Nature*, **292**: 81–82 (1981).

55) Shaanan, B.: Structure of human oxyhemoglobin at 2.1 Å resolution. *J. Mol. Biol.*, **171**: 31–59 (1983).

56) Olson, J. S., Mathews, A. J., Rohlfs, R. J., Springer, B. A., Egeberg, K. D., Sligar, S. G., Tame, J., Renaud, J.-P. and Nagai, K.: The role of the distal histidine in myoglobin and haemoglobin. *Nature*, **336**: 265–266 (1998).

57) Springer B. A., Sligar, S. G., Olson, J. S. and Phillips Jr. G. N.: Mechanism of ligand recognition in myoglobin. *Chem. Rev.*, **94**: 699–714 (1994).

58) Chu, M. M. L., Castro, C. E. and Hathaway, G. M.: Oxidation of low-spin iron(III) porphyrins by molecular-oxygen-outer sphere mechanism. *Biochemistry*, **17**: 481–486 (1978).

59) Tsuchida, E., Nishide, H., Sato, Y. and Kaneda, M.: The preparation of protoheme mono-N[5-(2-methyl-1-imidazolyl)phenyl] amide and its oxygenation. *Bull. Chem. Soc. Jpn.*, **55**: 1890–1895 (1982).

60) Uno, T., Sakamoto, R., Tomisugi, Y., Ishikawa, Y. and Wilkinson, A.: Inversion of axial coordination in myoglobin to create a "proximal" ligand binding pocket. *Biochemistry*, **42**: 10191–10199 (2003).

61) Sharma, V. S., Schmidt, M. R. and Ranney, H. M.: Dissociation of CO from carboxyhemoglobin. *J. Biol. Chem.*, **251**: 4267–4272 (1976).

62) Imai, K., Morimoto, H., Kotani, M., Watari, H., Hirata, W. and Kuroda, M.: Studies on the function of abnormal hemoglobins I. An improved method for automatic measurement of the oxygen equilibrium curve of hemoglobin. *Biochim. Biphys. Acta.*, **200**: 189–197 (1970).

63) Steinmeier, R. C. and Parkhurst, L. J.: Kinetic studies on the five principal components of normal adult human hemoglobin. *Biochemistry*, **14**: 1564–1571 (1975).

64) Dougherty, T. J., Gomer, C. J., Henderson, B. W., Jori, G., Kessel, D., Korbelik, M., Moan, J. and Peng, Q.: Photodynamic therapy. *J. Natl. Cancer Inst.*, **90**: 889–905 (1998).

65) Sharman, W. M., Allen, C. M. and Lier, J. E.: Photodynamic therapeutics: basic principles and clinical applications. *Drug Discov. Today*, **4**: 507–517 (1999).

66) Sternberg, E. D., Dolphin, D. and Bruckner, C.: Porphyrin-based photosensitizers for use in photodynamic therapy. *Tetrahedron*, **54**: 4151–4202 (1998).

67) Dougherty, T. J.: Studies on the structure of porphyrins contained in Photofrin-II. *Photochem. Photobiol.*, **46**: 569–573 (1987).

68) Aveline, B., Hasen, T. and Redmond, R. W.: Photophysical and photosensitizing properties of benzoporphyrin derivative monoacid ring A (BPD-MA). *Photochem. Photobiol.*, **59**: 328–335 (1994).

69) Kato, H., Furukawa, K., Sato, M., Okunaka, T., Kusunoki, Y., Kawahara, M., Fukuoka, M., Miyazawa, T., Yana, T., Matsui, K., Shiraishi, T. and Horinouchi, H.: Phase II clinical study of photodynamic therapy using mono-L-aspartyl chlorine e6 and diode laser for early superficial squamous cell carcinoma of the lung. *Lung Cancer*, **42**: 103–111 (2003).

70) Kennedy, J. C., Pottier, R. H. and Pross, D. C.: Photodynamic therapy with endogeneous protoporphyrin IX: basic principles and present clinical experience. *J. Photochem. Photobiol. B*, **6**: 143–148 (1990).

71) Lopez, R. F. V., Lange, N., Guy, R. and Bentley, M. V. L. B.: Photodynamic therapy of skin cancer: controlled drug delivery of 5-ALA and its esters. *Drug Deliver. Rev.*, **56**: 77–94 (2004).

72) Arbogast, J. W., Darmanyan, A. P., Foote, C. S., Rubin, Y., Diederich, F. N., Alvarez, M. M., Anz, S. J. and Whetten, R. L.: Photophysical properties of C_{60}. *J. Phys. Chem.*, **95**: 11–12 (1991).

73) Guldi, D. M. and Prato, M.: Excited-state properties of C_{60} fullerene derivatives. *Acc. Chem. Res.*, **33**: 695–703 (2000).

74) Nakamura, E. and Isobe, H.: Functionalized fullerene in water. The first 10 years of their chemistry, biology, and nanooscience. *Acc. Chem. Res.*, **36**: 807–815 (2003).

75) Andersson, T., Nilsson, K., Sundahl, M., Westman, G. and Wennerstrom, O.: C_{60} embedded in γ-cyclodextrin: a water-soluble fullerene. *Chem. Commun.*, 604–606 (1992).

76) Yoshida, Z., Takekuma, H., Takekuma, S. and Matsubara, Y.: Molecular recognition of C_{60} with γ-cyclodextrin. *Angew. Chem. Int. Ed.*, **33**: 1597–1599 (1994).

77) Benyamini, H., Shulman-Peleg, A., Wolfson, H. J., Belgorodsky, B., Fadeev, L. and Gozin, M.: Formation and characterization of stable human serum albumin-tris-malonic acid [C_{60}]fullerene complex. *Bioconjugate Chem.*, **17**: 378–386 (2006).

78) Anderson, J. L., An, Y.-Z., Rubin, Y. and Foote, C. S.: Photophysical characterization and single oxygen yield of a dihydrofullerene. *J. Am. Chem. Soc.*, **116**: 9763–9764 (1994).

79) Wilkinson, F., Helman, W. P. and Rossa, A. B.: Quantum yields for the photosensitized formation of the lowest electronically excited singlet-state of molecular-oxygen in solution, *J. Phys. Chem. Ref. Data*, **22**: 113–262 (1993).

80) Hamano, T., Okuda, K., Mashino, T., Hirobe, M., Arakane, K., Ryu, A., Mashiko, S. and Nagano, T.: Singlet oxygen production from fullerene derivatives: effect of sequential functionalization of the fullerene core. *Chem. Commun.*, 21–22 (1997).

81) Prat, F., Stackow, R., Bernstein, R., Qian, W., Rubin, Y. and Foote, C. S., Triplet-state properties and singlet oxygen generation in a homologous series of functionalized fullerene derivatives. *J. Phys. Chem. A*, **103**: 7230–7235 (1999).

82) Tanielian, C., Wolff, C. and Esch, M.: Singlet oxygen production in water: aggregation and charge-transfer effects. *J. Phys. Chem.*, **100**: 6555–6560 (1996).

83) Kobayashi, K.: Summary of recombinant human serum albumin development. *Biologicals*, **34**: 55–59 (2006).

総　説

ヒト血清アルブミンを用いた機能分子・材料の創製

Synthesis of Functional Molecules and Materials Based on Human Serum Albumin

小松 晃之[1,2]，屈　雪[1]，土田 英俊[1]，中川 晶人[1]

Teruyuki Komatsu[1,2], Xue Qu[1], Eishun Tsuchida[1], Akito Nakagawa[1]

和文抄録

筆者らはヒト血清アルブミン（HSA）の多分子結合能を利用して，その内部に機能性分子を包接させる方法や，さらにはHSAと高分子電解質の交互積層膜を多孔性膜の細孔内で作成する方法により，自然界には見ることのできないユニークな機能分子・材料を創製してきている．HSAに鉄テトラフェニルポルフィリン誘導体（FeP）を包接させたHSA-FeP複合体は生理条件下で酸素を可逆的に結合解離できる人工酸素運搬体となり，遺伝子組換えアルブミン（rHSA）にヘモグロビンの活性中心である鉄プロトポルフィリン（heme）を結合させたrHSA-heme錯体も酸素吸脱着のできる人工ヘム蛋白質となる．一方，HSA－亜鉛プロトポルフィリン錯体は水の光還元による水素発生反応の増感剤として作用し，HSA－カルボキシフラーレン複合体は一重項酸素生成の光増感剤として腫瘍光線力学療法への応用が期待されている．さらに，多孔性ポリカーボネート膜をテンプレートとした鋳型内交互積層法により，HSAからなる中空シリンダー構造のナノチューブが合成できる．これらの新機能分子・材料の特徴と応用展開について，最近の話題を紹介する．

Abstract

We have synthesized unique functional molecules and materials based on human serum albumin (HSA), which have never seen in nature, by means of incorporation of functional ligands into the protein or fabrication of layer-by-layer assembly in the nanoporous membrane. HSA incorporating iron (II) tetraphenylporphyrin derivative (FeP) (HSA-FeP) is an artificial O_2 carrier which can reversibly binds and release O_2 under physiological conditions. Recombinant HSA complexed with a natural iron (II) protoporphyrin IX (heme) (rHSA-heme) also acts as O_2 transport hemoprotein. On the other hand, HSA complexed with a zinc (II) protoporphyrin IX functions as a photosensitizer for H_2 evolution from water, and HSA-carboxy fullerene hybrid produces singlet O_2 by visible light irradiation; it may be used as a sensitizer in photodynamic cancer therapy. Furthermore, HSA nanotubes are prepared by layer-by-layer deposition technique using porous polycarbonate membrane template. We highlight recent development and applications of these functional molecules and materials.

Keywords

Human serum albumin, albumin-heme, oxygen carrier, red blood cell substitute, photosensitizer, nanotubes

1．はじめに

ヒト血清アルブミン（HSA）は血清蛋白質の約60％を占める補欠分子族を持たない単純蛋白質（分子量：66,500）であり，血流中ではコロイド浸透圧維持のほか，各種内因性・外因性物質（脂肪酸，ヘミン，ビリルビン，金属イオン，ホルモン，NO，薬物）の運搬・貯蔵，pH緩衝作用，エステラーゼ活性などの役割を担っている[1-3]．1992年，米国国立航空宇宙局（NASA）のCarterらはHSAの高分解能X線結晶構造解析（分解能：2.8 Å）に成功し，その三次元構造の全容を明らかにした[4]．585個のアミノ酸からなる一本鎖ポリペプチドは17個のジスルフィド結合を介してハート形に折りたたまれ（長径：約8 nm，厚み：約3 nm），相同性の高い3つのドメインI～III

(1) 早稲田大学 理工学術院 総合研究所（理工学研究所） 〒169-8555 東京都新宿区大久保3-4-1 Research Institute for Science and Engineering, Waseda University, 3-4-1 Okubo, Shinjuku-ku, Tokyo 169-8555, Japan

(2) 科学技術振興機構さきがけ 〒332-0012 埼玉県川口市本町4-1-8 PRESTO, Japan Science and Technology Agency (JST), 4-1-8 Honcho, Kawaguchi-shi, Saitama 332-0012, Japan

論文受付 2009年5月7日　論文受理 2009年5月22日

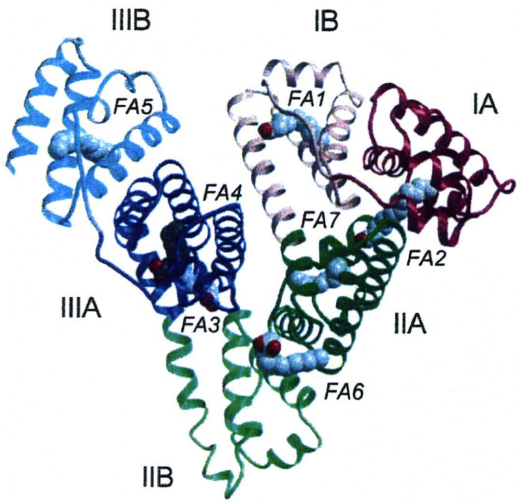

Fig. 1. Structure of HSA with seven myristic acids (PDB 1e7g). The protein secondary structure is shown schematically and the domains are colored (I; red, II; green, III; blue). The A and B subdomains are depicted in dark and light shades, respectively. The fatty acid binding sites are represented from FA1 to FA7 in italics.

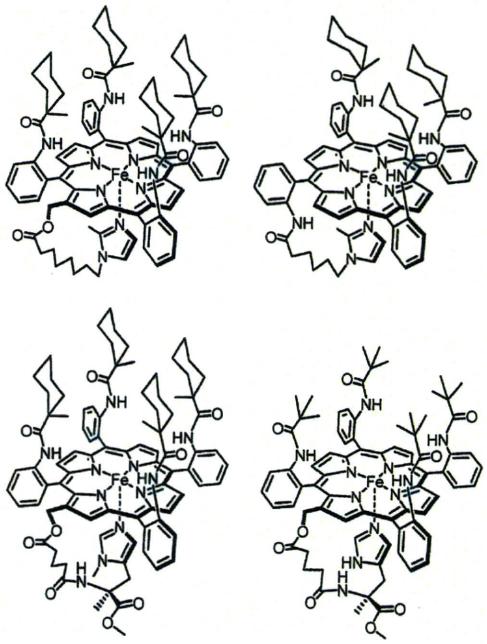

Fig. 2. Chemical formula of typical FeP molecules that can be incorporated into HSA to form HSA-FeP hybrid.

を構成している（各ドメインはさらに２つのサブドメインA，Bに分けられる．Fig. 1）．Sudlowらが提唱した古典的なHSAの薬物結合サイトI（ワルファリン，インドメタシンなど）はサブドメインIIA，薬物結合サイトII（ジアゼパム，イブプロフェンなど）はサブドメインIIIAに相当する[5]．

一方，HSAは遺伝子組換え技術により大量発現が可能な蛋白質である[6]．近年，その多分子結合能と高い生産性に注目が集まり，HSAに金属錯体を包接させた人工蛋白質の構築が盛んになってきている．例えば，GrossらはHSAにマンガンコロールを結合させた複合体を調製し，スルフィドの立体選択的酸化触媒として利用した[7]．また，ReetzらはHSAに銅フタロシアニンを結合させた複合体が，Diels-Alder反応に有用であることを明らかにした[8]．

本稿では，酸素運搬体，光増感剤から，蛋白質ナノチューブまで，著者らが進めているHSAを利用した新しい機能分子・材料の創製と応用について最近の話題を紹介したい．

２．アルブミン－脂肪酸複合体の結晶構造解析

HSAの最もよく知られたリガンドに脂肪酸がある．1998年，CurryらはHSA－脂肪酸複合体のX線結晶構造解析に初めて成功し，中・長鎖脂肪酸の結合サイト（FAサイト）を特定した[9,10]．HSAには全ての脂肪酸に共通する７個のサイトがあり（Fig. 1），FAサイト１，４，５，７は各サブドメインの中央に，FAサイト２，３は二つのドメインの境界面に，そしてFAサイト６は二つのサブドメインの境界面に位置する．FAサイト１－５では，脂肪酸の末端カルボキシル基が塩基性または極性アミノ酸残基と相互作用することによりしっかりと固定されている．これら５つのうちどこが最も親和性の強い部位なのか，結晶構造からは判定できない．組換えHSAの詳細な^{13}C-NMRスペクトル測定から，FAサイト２，４，５が親和力の強いサイトであることが明らかにされた[11]．７つのFAサイト全てに脂肪酸が結合すると，HSA全体の分子形態はダイナミックに変化する．特にドメイン間に存在するFAサイト２，３への結合は，ドメインIIを軸として大きな形態変化を誘起した．HSAの二次構造はα-ヘリックスが67％，β構造が０％である．古くから脂肪酸などのリガンド結合によりHSAの二次構造が変化するという報告があるが，リガンド結合後も二次構造に変化はないことが結晶学的に示された．Curryらはその後も各種HSA－リガンド複合体の結晶構造解析を系統的に進め，多くの複合体について構造を解明している[12-14]．現在Protein Data Bank（PDB）に登録済みのHSA－リガンド複合体のデータ47件のうち，37件はCurryらによるものである．

３．アルブミン－合成ヘム複合体（人工酸素運搬体）

我々は独自の分子設計により合成した鉄テトラフェニルポルフィリン誘導体（合成ヘム：FeP）をHSAに包接させたアルブミン－ヘム（HSA-FeP）複合体が，生理条件下でヘモグロビン（Hb）と同じように酸素を吸脱着できることを見出した[15-18]．これまでに約30種類以上のFeP（Fig. 2）を合成し，その酸素結合能とヘム構造の相関を整理してきている[19-22]．酸素錯体の安定度は天然のミオグロビン（Mb）を上回り，酸素親和性（P_{50}）は0.1 Torrから230 Torrまで所望の値に揃えることができる．つまり，適用に応じた製剤の選択が可能となっている．HSA-FeP溶液の血液適合性は高く，血液凝固系，補体系，血小板の活性化に対しても影響を及ぼさない[23]．室温で２年以上の棚置保存が可能で，その間酸素結合パラメーターに変

化はない[24]．脱血交換試験（ラット，ビーグル犬）から出血ショック状態からの蘇生効果，生体内における酸素輸送能が証明されている[25,26]．体内投与後も修飾Hb製剤に見られるような血管内皮細胞からの漏出，一酸化窒素捕捉に伴う血管収縮，血圧亢進は全く観測されない[27]．これはHSAの表面電荷が負に帯電しているため血管から漏れ出しにくいことに起因すると考えられており，本製剤の最大の利点となっている．

一般に悪性腫瘍は放射線療法や化学療法に抵抗性を示し，その原因の一つとして腫瘍組織内低酸素細胞（hypoxic cell）の存在があげられる．細胞の異常な増殖により新生血管の生成が追いつかない湿潤性腫瘍細胞では，十分な血流および酸素化が得られず，それが治療の妨げとなっている．HSA-FeP溶液を腫瘍組織の患部近傍へ投与し，腫瘍組織内低酸素細胞の酸素化を試みたところ，患部の酸素分圧は投与前の2.5倍に増大した[28]．これは，従来報告されている修飾Hb製剤を用いた処置に比べて格段に高く[29]，粒子径の小さいHSA-FePが腫瘍内部へ容易に到達できるためと考えられる．実際に放射線療法と併用した結果，HSA-FeP投与による抗癌作用の顕著な増強効果が認められた[30]．また，HSA-FePの分子表面をポリ（エチレングリコール）で被覆すると，血中滞留時間が大幅に延長されることも明らかにされている[31,32]．

4．遺伝子組換えアルブミンープロトヘム錯体（人工酸素運搬体）

アルブミン一合成ヘム複合体の酸素結合部位は，精密に分子設計された鉄テトラフェニルポルフィリン誘導体（FeP）であり，得られたHSA-FeP複合体が酸素を可逆的に結合解離できることは，錯体化学的に見れば設計通りの機能発現といえる．HSAを用いた人工酸素運搬体開発における究極の挑戦は，やはりHbの酸素結合部位であるヘム鉄［鉄プロトポルフィリンIX（プロトヘム，heme)］（Fig. 3a）を用いた製剤の確立であろう．2004年，我々は遺伝子組換え技術を用いてアミノ酸の一部を改変した組換えHSA（rHSA）にhemeを包接させたrHSA-heme錯体が，水中で酸素を吸脱着できることを見出した[33]．

溶血により血中に放出されたメトHbから解離した鉄（III）プロトポルフィリンIX（hemin）は，通常ヘモペキシンと呼ばれる糖蛋白質に捕捉されるが[34]，ヘモペキシンの血中濃度は約17μMと低いため，遊離heminの多くは一旦HSAに結合し肝臓へと運ばれる．HeminがHSAに捕捉されることは昔から知られていた．1938年，Fairelyはheminと相互作用する血清蛋白質がHSAであることを発見し，その複合体をhemalbuminと名付けた[35]．それ以来，このHSA-hemin錯体は，何らかの生理作用があるのではないかと研究者達の関心の的となってきた．1975年，Muller-EberhardらによりHSA-hemin錯体の吸収スペクトルが報告され，heminの中心鉄にアミノ酸残基が軸配位した高スピンヘム錯体構造が推定された[36]．また，1980年にはBermanらがHSAとheminの結合定数（K：$1.1\times10^{8}\ M^{-1}$）を決定[37]，この値は脂肪酸に比べて約100倍高く，heminがHSAに強く結合することが明確となった．

2002年，Carterと我々のグループは独立にHSA-hemin錯体のX線結晶構造解析に成功し，heminがHSAのサブドメインIB内の疎水ポケットに結合していることを明らかにした[38,39]．この部位は，脂肪酸のFAサイト1に相当する．heminの中心鉄にはチロシン（Tyr)-161のフェノレート酸素が軸配位し，二つのプロピオン酸残基は，三つの塩基性アミノ酸残基（リシン，ヒスチジン，アルギニン）と相互作用していることがわかった（Fig. 3b）．よく知られているようにMbのヘムポケット内では，ヘム中心鉄にヒスチジン（His)-93が軸配位し，そのトランス側（第6配位座）に酸素分子が結合する（Fig. 3c）．さらに，配位酸素側にはもう一つのHis-64が遠位塩基として存在し，酸素錯体を安定化している．ここで両者を見比べてみると，誰もがその構造類似性に気づくであろう．しかし，残念ながらHSA-hemin錯体の中心鉄を鉄（II）に還元して酸素を吹き込んでみても，酸素錯体は得られない[33]．それは軸配位子がHisではないためである．HSA-hemin錯体が血中で何らかの役割をはたしているのではないかという期待とは裏腹に，むしろHSAはhemin分子の活性を巧みに抑え込んでいたのである．しかしながら，hemeが疎水的な分子空間に配置された構造はMbのヘムポケットと共通しているので，それならばHSAの場合でもヘム鉄の配位圏内（サブドメインIB）にHisが存在すれば，酸素錯体ができるのではないかと考えた．そこで遺伝子組

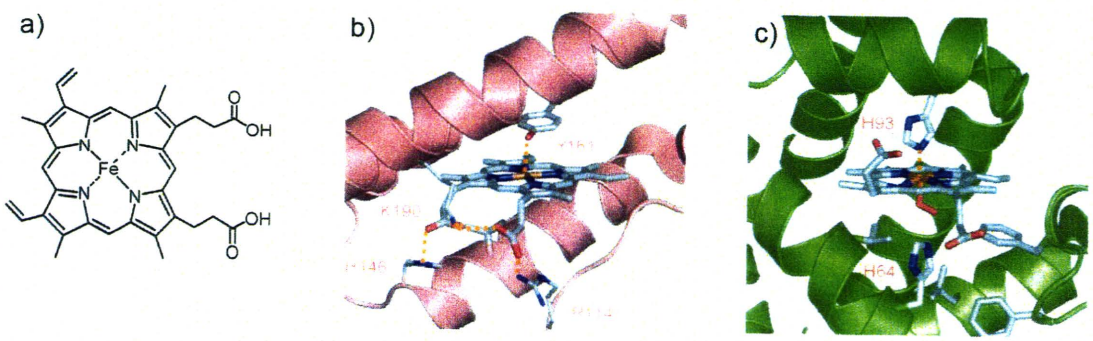

Fig. 3. (a) Chemical formula of iron (II) protoporphyrin IX (heme). Heme pocket structures of (b) HSA-hemin complex (PDB 1o9x) and (c) oxy-Mb (pdb 1mbo).

換え技術を用いて，イソロイシン（Ile)-142位置へ近位塩基として働くHisを変異導入し，さらに中心鉄に軸配位しているTyr-161を疎水性アミノ酸（ロイシン（Leu））に変換したところ，その組換えHSA-heme［rHSA（I142H/Y161L)-heme］錯体は，室温で酸素を吸脱着することができた[33,40]．rHSAとhemeから構成される酸素輸送人工ヘム蛋白質の初めての例である．そこで，酸素結合パラメーターを詳細に解析した．rHSA（I142H/Y161L)-heme錯体の$P_{1/2}$は18 Torr（22℃）であり，Hb，Mb，ヒト赤血球の値に比べて高い（酸素親和性は低い）．rHSA（I142H/Y161L)-heme錯体の低い酸素親和性は，速度論的には大きな解離速度定数（k_{off}）に起因した[33,40]．rHSAの中ではhemeを取り巻く分子環境が疎水的であるためにk_{off}が高く，酸素親和性が低く抑えられているのである．

このように酸素錯体は得られたものの，実際にrHSA（I142H/Y161L)-heme錯体を人工酸素運搬体として利用するためには，その酸素親和性をHbや赤血球の値に近づけなければならない．そこで，第三の変異を導入することにより，酸素親和性を上げる工夫を行った．前述したように，HbやMbのヘムポケット内には酸素配位座側にHis-64が遠位塩基として存在し，酸素親和性の増大に寄与している[41,42]．我々はrHSAの場合も，酸素配位座側の適当な位置に遠位塩基を導入すれば，酸素親和性が上昇するのではないかと考えた．分子シミュレーションの結果から配位酸素直上のLeu-185を選定し，そこへ遠位塩基としてのアスパラギン（Asn）を導入した［rHSA（I142H/Y161L/L185N)］[43]．rHSA（I142H/Y161L/L185N)-heme錯体（Fig. 4）の可視吸収スペクトルは，窒素雰囲気下では鉄（II）5配位高スピン錯体の形成を示し，そこへ酸素を通気すると速やかに酸素錯体型へと移行した．$P_{1/2}$は1 Torr（22℃）となり，酸素親和性はもとの二重変異体に比べて18倍も上昇した．Asnの導入によりヘムポケットの極性が増大しk_{off}が減少した結果，酸素親和性が上がったものと考えられる．rHSA（I142H/Y161L/L185N)-heme錯体は，Hbと同等の酸素親和性を有する人工ヘム蛋白質となった．つまり我々は，本来補欠分子族すらもたない単純蛋白質のHSAに，酸素結合能を付与することに成功したばかりでなく，ヘムポケットの微小空間を部位特異的アミノ酸置換により最適化することで，酸素親和性のコントロールを実現したのである．

ごく最近，酸素配位座側にあるアルギニン（Arg)-186を疎水性アミノ酸に変換すると，酸素親和性がヒト赤血球と同等値に調整できることを見出した[13]．rHSA-heme錯体は天然のプロトヘムを活性中心とする，いわば“酸素輸送のできる赤色の血清蛋白質”である．臨床利用可能な赤血球代替物として，現在実用化に向けた努力が進められている．

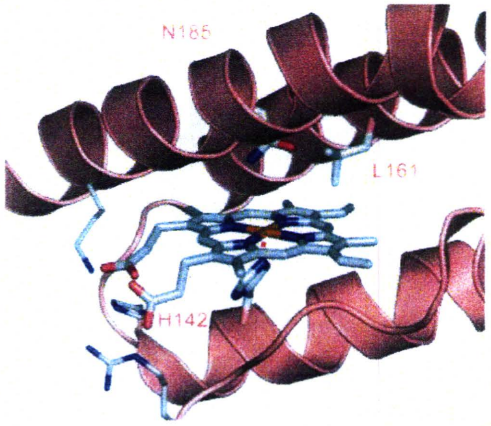

Fig. 4. Structural model of the heme pocket in rHSA (I142H/Y161L/L185N)-heme complex.

5．アルブミン－亜鉛プロトポルフィリン錯体（水素発生の光増感剤）

ポルフィリン化合物の最大の魅力は，その中心金属を変えることにより多彩な機能を発揮できる点にある．特に可視光領域に大きな吸収帯を持つ特徴を生かして，光反応の増感剤として広く利用されている．しかし，鉄ポルフィリン錯体は光励起状態の寿命がきわめて短いため，一般的には光反応の増感剤には適さず，励起寿命の長い亜鉛錯体が用いられる．

水素（H_2）は二酸化炭素排出のない近未来のクリーンエネルギーである．Grätzelらは亜鉛テトラメチルピリジニウムポルフィリンをメチルビオロゲン（MV^{2+}）／白金コロイド／EDTA水溶液に加え可視光照射すると，水の光還元反応が進行し水素が得られることを見出した[44]．もしプロトポルフィリンIX（PP）が水の光還元に利用できれば，天然物質を増感剤とした水素発生システムが確立できることになる．しかし，亜鉛プロトポルフィリンIX（ZnPP）は水に不溶で，そのまま使用することは難しい．そこで，ZnPPをHSAに包接させることによりHSA-ZnPP錯体とし，水の光還元反応への応用を試みた．HSA-ZnP錯体水溶液にMV^{2+}を加え，アルゴン雰囲気下でレーザーフラッシュ（532 nm）を照射すると，ZnPの励起三重項状態からMV^{2+}への電子移動反応が観測された[45]．続いて，白金コロイド，犠牲試薬としてのトリエタノールアミンを加え可視光照射してみると，速やかに水の還元が起こり溶液中から水素が発生した（Fig. 5）．水素発生効率は亜鉛テトラメチルピリジニウムポルフィリンを用いた場合よりも高い．つまり，HSA-ZnPP錯体は水の光還元反応における有効な増感剤として機能する．

この結果は，アルブミン－ポルフィリン錯体においてポルフィリンの中心金属を変えることにより，様々な機能を持った人工蛋白質が創製できることを示唆している．

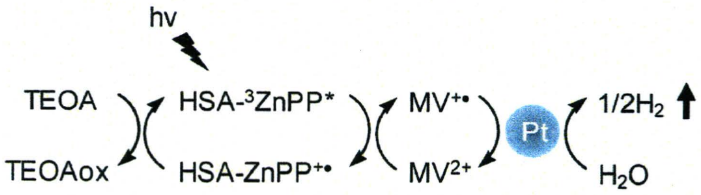

Fig. 5. Reaction scheme of photoreduction of water to hydrogen using HSA-ZnP complex.

6．アルブミン－フラーレン複合体（光線力学療法の増感剤）

金属ポルフィリン以外の機能性分子でもHSAに包接させれば，新しい人工蛋白質が合成できるはずである．そこで，HSAにフラーレン誘導体を包接させたアルブミン－フラーレン複合体を調製し，その構造，光物性，光線力学療法（photodynamic therapy: PDT）における増感剤としての可能性について検討した．現在，よく知られているPDTの光増感剤には，ヘマトポルフィリンの誘導体であるフォトフリン[46,47]，プロトポルフィリンの前駆体である5-アミノレブリン酸[48]，またクロリン誘導体であるビスダイン[49]などがある．これらのポルフィリン誘導体に比べ，フラーレンC_{60}は高い光安定性を持ち，一重項酸素生成の量子収率が高いことから，PDTの新しい増感剤として期待されている[50-52]．

HSAにカルボキシフラーレン（CF，Fig. 6a）を包接させたHSA-CF複合体はきわめて安定で，その水溶液は調製２年後でも沈殿・凝集など全く認められなかった（Fig. 6b）[53]．可視吸収スペクトル，HPLC，質量分析の結果から，HSAとCFが１：１で結合していること，さらに小角X線散乱測定から，CF結合後もHSAの分子径，表面電荷に変化はないことがわかった[53]．

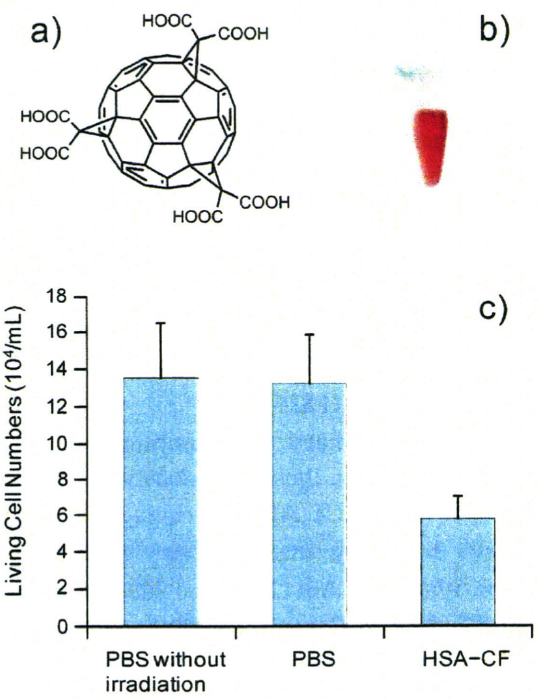

Fig. 6. (a) Chemical formula of carboxy-C_{60}-fullerene, (b) red colored solution of aqueous HSA-CF, and (c) living cell numbers of LY80 with HSA-CF and PBS after visible light irradiation (20 mW cm^{-2}, 2 h, 36 ± 1℃). Each value represents the mean ± SD (n = 4).

一般に色素分子を光励起すると，まず励起一重項状態を形成し，そこから項間交差により励起三重項状態へと遷移する．一重項酸素生成の有効な光増感剤となるためには，この励起三重項状態が安定でなければならない．HSA-CF複合体の励起三重項寿命は46 μsと長く，それはCFが蛋白質内部に固定されているため，励起種どうしによる消光が抑えられることによる．系内に酸素を共存させると，励起三重項状態から酸素分子へのエネルギー移動が観測された．生成する一重項酸素は1270 nmに蛍光を示すので，その強度から一重項酸素生成の量子収率が算出できる．HSA-CF複合体の量子収率は0.46であり，HSA-PP複合体やメチレンブルーと同程度であったことから[54]，本化合物が一重項酸素生成の有効な光増感剤として作用することがわかった．

続いてこの製剤の細胞毒性について検証した．腫瘍細胞（LY80）にHSA-CF水溶液を加え，まず暗所下でそれ自身に細胞毒性がないことを確認．その後ハロゲンランプを用いて光照射（２hr）すると，細胞数は43％にまで減少した（Fig. 6c）[53]．この結果はHSA-CF複合体がPDTの光増感剤として有効であることを示している．

7．アルブミンナノチューブ（分子捕捉剤，薬物運搬体，ナノリアクター）

ピキア酵母を用いた遺伝子組み換え体の量産体制が確立して以来，HSAは臨床利用はもちろんバイオマテリアルの有用な素材としても注目を集めている[6]．我々は最近，鋳型内交互積層法によりHSAからなる中空シリンダー構造のナノチューブを合成することに成功した[55-57]．HSAの等電点は4.8と低く，生理条件下では分子表面が負に帯電している．上述したようにHSAがHbに比べて血管外へ逸脱し難いのは，血管内皮細胞の外側にある基底膜との静電反発による．そこでまず正電荷を有する高分子電解質（例えば，ポリ-L-アルギニン（PLA）などのポリアミノ酸やポリエチレンイミンなど）を多孔性ポリカーボネート（PC）膜の細孔内に通過させ，続いてHSA水溶液を通過させる．この操作を繰り返しながら，細孔内壁にHSAの多重積層膜を作成し，最後にPC膜を溶解除去すると，HSAからなる均一で柔軟なナノチューブが得られる．孔径400 nmのPC膜にPLAとHSAを各３回ずつ通過させて作成した計６層構造からなるナノチューブの外径は約400 nm，内径は約300 nm，管壁厚は約50 nmとなる（Fig. 7）．鋳型内交互積層法（テンプレート合成）の利点は，

① 電荷を有する水溶性分子（蛋白質，生体分子，高分子電解質など）であれば，ナノチューブの素材になり得る（分子設計の自由度が高く，構成分子の選択範囲が広い）
② 鋳型となる多孔性膜の孔径および厚みの調節により，チューブの外径および長さを均一に制御することができる
③ 積層膜数の調節により，チューブの内径をナノメートルスケールで制御することができる
④ 複数の機能性分子を任意の順序で積層することにより，管壁構造を自由に分子設計できる
⑤ 他のナノチューブ合成法に比べ，調製が簡便，再現性が高く，低コスト，大型化が容易

などである．

得られたナノチューブの最大の特徴は，同重量の球状構造体

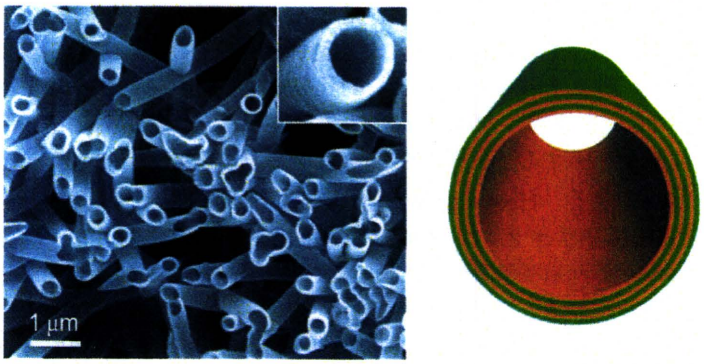

Fig. 7. SEM images of protein nanotubes comprised of $(PLA/HSA)_3$. Schematic illustration of the protein nanotubes prepared by template synthesis using layer-by-layer deposition technique.

に比べて比表面積が大きいことにある．HSAナノチューブの水分散液にHSAのリガンド（薬物など）を添加すると，ナノチューブ管壁に効率よく結合し，水中から速やかに除去される．HSAに結合しない分子は全く取り込まれないので，いつまでも水中に存在する．HbやMbを構成成分としてナノチューブを作成することもできるし[57]，HSA-FePからなるナノチューブは酸素を可逆的に吸脱着する[55]．また，最終層成分の選定だけで内孔に合目的な特性を付与することができるので，例えば最内層に加水分解酵素を配置したHSAナノチューブでは，内孔壁表面で基質の加水分解が進行する．逆に酵素合成により新物質を創り出すこともできる．まさにナノサイズのリアクターである．この場合，内孔以外の管壁を構成する蛋白質がHSAであることが肝要である．他にも鉄イオンの捕捉・貯蔵を担う球殻状蛋白質フェリチンからなるナノチューブも合成され，バイオナノデバイスとして磁化特性，半導体特性が検討されている．

管壁のみならず，チューブの一次元内孔空間にウイルスやリポソームなどの大きな生体超分子をサイズ選択的に捕捉することも可能である．中空シリンダーの両端開口部が自由に開閉できれば，従来のミセルやリポソームとは全く違う新しいドラッグキャリアの誕生にもつながるであろう．

8．おわりに

筆者らはヒト血清アルブミンの多分子結合能に着目し，その内部に機能性分子を取り込ませる方法により，数々の人工蛋白質を創製してきている．当初は酸素運搬体に焦点を絞った展開であったが，合成ヘムのみならず他の機能性分子も効率よく包接できることがわかり，水の還元による水素発生や一重項酸素生成の光増感剤となるアルブミンを開発した．実は多分子結合能のみならず，きわめて高い水溶性や光・熱に対する安定性といった血清蛋白質アルブミンならではの特徴が，これらの新物質系において重要な役割を果たしている．さらに，遺伝子組換え技術を駆使してアルブミンのアミノ酸配置を少しだけ変えてやると，機能制御が可能になることも明らかにした．X線結晶構造解析（生物物理学）にもとづいた部位特異的アミノ酸置換（分子生物学）を機能性アルブミン開発の分子設計に取り入れ，新しい方法論として定着させた．最近はアルブミンからなる中空シリンダー構造のナノチューブを合成し，その機能展開に力を入れているが，ここでもアルブミンの高い構造安定性が大きく貢献している．ウイルス捕捉，標的薬物の結合・放出，ナノリアクター，ナノバイオデバイスなど，多くの応用展開が期待される．

謝　辞

本総説は，日本学術振興会科学研究費補助金，科学技術振興機構戦略的創造研究推進事業“さきがけ”，厚生労働省科学研究費補助金の支援により推進された研究の成果である．遺伝子組換え蛋白質の合成，X線結晶構造解析はProf. Stephen Curry（Imperial College London）の協力のもと行われた．動物実験は小林紘一教授（慶大医），堀之内宏久准教授（慶大医）の協力を得て実施された．また，試料調製・生化学実験は小林　直（早大理工研），寺田裕美（早大理工研）が担当した．ここに記して謝意を表する．

引用文献

1. Peters T. All about Albumin: Biochemistry, Genetics and Medical Applications. San Diego: Academic Press, 1996; and references therein.
2. Kragh-Hansen U. Molecular aspects of ligand binding to serum albumin. Pharmacol Rev 1981;33:17-53.
3. Kragh-Hansen U. Structure and ligand-binding properties of human serum-albumin. Danish Med Bull 1990;37:57-84.
4. He XM, Carter DC. Atomic structure and chemistry of human serum albumin. Nature 1992;358:209-215.
5. Sudlow G, Birkett DJ, Wade DN. The characterization of two specific drug binding sites on human serum albumin. Mol Pharmacol 1975;11:824-832.
6. Kobayashi K. Summary of recombinant human serum albumin development. Biologicals 2006;34:55-59.
7. Mahammed A, Gross Z. Albumin-conjugated corrole metal complexes: extremely simple yet very efficient biomimetic oxidation Systems. J Am Chem Soc 2005;127:2883-2887.
8. Reetz MT, Jiao N. Copper-phthalocyanine conjugates of serum albumins as enantioselective catalysts in Diels-Alder reactions. Angew Chem Int Ed 2006;45:2416-2419.
9. Curry S, Madelkow H, Brick P, Franks N. Crystal structure of human serum albumin complexed with fatty acid reveals an asymmetric distribution of binding sites. Nat Struct Biol 1998;5:827-835.
10. Curry S, Brick P, Franks N. Fatty acid binding to human serum albumin: new insights from crystallographic studies. Biochim Biophys Acta 1999;1441:131-140.
11. Simard JR, Zunszain PA, Hamilton JA, Curry S. Location of high and low affinity fatty acid binding sites on human

serum albumin revealed by NMR drug-competition analysis. J Mol Biol 2006;361:336-351.
12. Petitpas I, Petersen CE, Ha CE, Bhattacharya AA, Zunszain PA, Ghuman J, Bhagavan NV, Curry S. Structural basis of albumin-thyroxine interactions and familial dysalbuminemic hyperthyroxinemia. Proc Natl Acad Sci USA 2003;100:6440-6445.
13. Ghuman J, Zunszain PA, Petotpas I, Bhattacharya AA, Otagiri M, Curry S. Structural basis of the drug-binding specificity of human serum albumin. J Mol Biol 2005;353:38-52.
14. Zunszain PA, Ghuman J, McDonagh AF, Curry S. Crystallographic analysis of human serum albumin complexed with 4Z,15E-birirubin-IXα. J Mol Biol 2008;381: 394-406.
15. Komatsu T, Hamamatsu K, Wu J, Tsuchida E. Physicochemical properties and O_2-coordination structure of human serum albumin incorporating tetrakis (o-pivalamido) phenylporphinatoiron (II) derivatives. Bioconjugate Chem 1999;10:82-86.
16. Tsuchida E, Komatsu T, Mastukawa Y, Hamamatsu K, Wu J. Human serum albumin incorporating tetrakis (o-pivalamido) phenylporphinatoiron (II) derivative as a totally synthetic O_2-carrying hemoprotein. Bioconjugate Chem 1999;10:797-802.
17. Komatsu T, Matsukawa Y, Tsuchida E. Kinetics of CO and O_2 binding to human serum albumin-heme hybrid. Bioconjugate Chem 2000;11:772-776.
18. Komatsu T, Matsukawa Y. Tsuchida E. Reaction of nitric oxide with synthetic hemoprotein, human serum albumin incorporating tetraphenylporphinatoiron (II) derivatives. Bioconjugate Chem. 2001;12:71-75.
19. Komatsu T, Okada T, Moritake M, Tsuchida E. O_2-binding properties of double-sided porphinatoiron (II) s with polar substituents and their human serum albumin hybrids. Bull Chem Soc Jpn 2001;74:1695-1702.
20. Komatsu T, Matsukawa Y, Tsuchida E. Effect of heme structure on O_2-binding properties of human serum albumin-heme hybrids: intramolecular histidine coordination provides a stable O_2-adduct complex. Bioconjugate Chem 2002;13:397-402.
21. Nakagawa A, Komatsu T, Iizuka M, Tsuchida E. Human serum albumin hybrid incorporating tailed porphyrinatoiron (II) in the $\alpha,\alpha,\alpha,\beta$-conformer as an O_2-binding site. Bioconjugate Chem 2006;17:146-151.
22. Nakagawa A, Komatsu T, Iizuka M, Tsuchida E. O_2 binding to human serum albumin incorporating iron porphyrin with a covalently linked methyl-L-histidine isomer. Bioconjugate Chem 2008;19:581-584.
23. Komatsu T, Huang Y, Wakamoto S, Abe H, Fujihara M, Azuma H, Ikeda H, Yamamoto H, Horinouchi H, Kobayashi K, Tsuchida E. Influence of O_2-carrying plasma hemoprotein "albumin-heme" on complement system and platelet activation in vitro and physiological responses to exchange transfusion. J Biomed Mater Res 2007;81A:821-826.
24. Tsuchida E, Komatsu T, Yanagimoto T, Sakai H. Preservation stability and in vivo administration of albumin-heme hybrid solution as an entirely synthetic O_2-carrier. Polym Adv Technol 2002;13:845-850.
25. Tsuchida E, Komatsu T, Hamamatsu K, Matsukawa Y, Tajima A, Yoshizu A, Izumi Y, Kobayashi K. Exchange transfusion of albumin-heme as an artificial O_2-infusion into anesthetized rats: physiological responses, O_2-delivery and reduction of the oxidized hemin sites by red blood cells. Bioconjugate Chem 2000;11:46-50.
26. Komatsu T, Yamamoto H, Huang Y, Horinouchi H, Kobayashi K, Tsuchida E. Exchange transfusion with synthetic oxygen-carrying plasma protein "albumin-heme" into an acute anemia rat model after seventy-percent hemodilution. J Biomed Mater Res 2004;71A:644-651.
27. Tsuchida E, Komatsu T, Matsukawa Y, Nakagawa Y, Sakai H, Kobayashi K, Suematsu M. Human serum albumin incorporating synthetic heme: red blood cell substitute without hypertension by nitric oxide scavenging. J Biomed Mater Res 2003;64A:257-261.
28. Kobayashi K, Komatsu T, Iwamaru A, Matsukawa Y, Watanabe M, Horinouchi H, Tsuchida E. Oxygenation of hypoxia region in solid tumor by administration of human serum albumin incorporating synthetic hemes. J Biomed Mater Res 2003;64A:48-51.
29. Linberg R, Conover CD, Shum KL, Shorr RGL. Increased tissue oxygenation and enhanced radiation sensitivity of solid tumors in rodents following polyethylene glycol conjugated bovine hemoglobin administration. In Vivo 1998;12:167-174.
30. Horinouchi H, Yamamoto H, Komatsu T, Huang Y, Tsuchida E, Kobayashi K. Enhanced radiation response of a solid tumor with the artificial oxygen carrier 'albumin-heme'. Cancer Sci 2008;99:1274-1278.
31. Huang Y, Komatsu T, Wang RM, Nakagawa A, Tsuchida E. Poly (ethylene glycol)-conjugated human serum albumin including iron porphyrins: surface modification improves the O_2-transporting ability. Bioconjugate Chem 2006;17:393-398.
32. Huang Y, Komatsu T, Yamamoto H, Horinouchi H, Kobayashi K, Tsuchida E. PEGylated albumin-heme as an oxygen-carrying plasma expander: exchange transfusion

into acute anemia rat model. Biomaterials 2006;27:4477-4483.
33. Komatsu T, Ohmichi N, Zunszain PA, Curry S, Tsuchida E. Dioxygenation of human serum albumin having a prosthetic heme group in a tailor-made heme pocket. J Am Chem Soc 2004;126:14304-14305.
34. Paoli M. Anderson BF, Baker HM, Morgan WT, Smith A, Baker EN. Crystal structure of hemopexin reveals a novel high-affinity heme site formed between two β-propella domains. Nat Struct Biol 1999;6:926-931.
35. Fairley NH. Methemalbumin (pseudo-methemoglobin). Nature 1938;142:1156-1157.
36. Muller-Eberhard U, Morgan WT. Porphyrin-binding proteins in serum. Ann NY Acad Sci 1975;244:624-650.
37. Adams PA, Berman MC. Kinetics and mechanism of the interaction between human serum albumin and monomeric haemin. Biochem J 1980;191:95-102.
38. Wardell M, Wang Z, Ho JX, Robert J, Ruker F, Rubel J, Carter DC. The atomic structure of human serum methemalbumin at 1.9 Å. Biochem Biophys Res Commun 2002;291:813-819.
39. Zunszain PA, Ghuman J, Komatsu T, Tsuchida E, Curry S. Crystal structural analysis of human serum albumin complexed with hemin and fatty acid. BMC Struct Biol 2003;3:6.
40. Komatsu T, Ohmichi N, Nakagawa A, Zunszain PA, Curry S, Tsuchida E. O_2 and CO binding properties of artificial hemoproteins formed by complexing iron protoporphyrin IX with human serum albumin mutants. J Am Chem Soc 2005;127:15933-15942.
41. Phillips SEV, Schoenborn BP. Neuteon diffraction reveals oxygen-histidine hydrogen bond in oxymyoglobin. Nature 1981;292:81-82.
42. Shaanan B. Structure of human oxyhemoglobin at 2.1 Å resolution. J Mol Biol 1983;171:31-59.
43. Komatsu T, Nakagawa A, Zunszain PA, Curry S, Tsuchida E. Genetic engineering of the heme pocket in human serum albumin: modulation of O_2 binding of iron protoporphyrin IX by variation of distal amino acids. J Am Chem Soc 2007;129:11286-11295.
44. Kalyanasundaram K, Grätzel M. Light induced redox reactions of water soluble porphyrins, sensitization of hydrogen generation from water by zincporphyrin derivatives. Helv Chim Acta 1980;63:478-485.
45. Komatsu T, Wang RM, Zunszain PA, Curry S, Tsuchida E. Photosensitized reduction of water to hydrogen using human serum albumin complexed with zinc-protoporphyrin IX. J Am Chem Soc 2006;128:16297-16301.
46. Dougherty TJ. Studies on the structure of porphyrins contained in Photofrin-II. Photochem Photobiol 1987;46:569-573.
47. Dougherty TJ, Gomer CJ, Henderson BW, Jori G, Kessel D, Korbelik M, Moan J, Peng Q. Photodynamic therapy. J Natl Cancer Inst 1998;90:889-905.
48. Lopez RFV, Lange N, Guy R, Bentley MVLB. Photodynamic therapy of skin cancer: controlled drug delivery of 5-ALA and its esters. Drug Deliver Rev 2004;56:77-94.
49. Aveline B, Hasen T, Redmond RW. Photophysical and photosensitizing properties of benzoporphyrin derivative monoacid ring A (BPD-MA). Photochem Photobiol 1994;59:328-335.
50. Guldi DM, Prato M. Excited-state properties of C_{60} fullerene derivatives. Acc Chem Res 2000;33:695-703.
51. Arbogast JW, Darmanyan AP, Foote CS, Rubin Y, Diederich FN, Alvarez MM, Anz SJ, Whetten RL. Photophysical properties of C_{60}. J Phys Chem 1991;95:11-12.
52. Anderson JL, An YZ, Rubin Y, Foote CS. Photophysical characterization and single oxygen yield of a dihydrofullerene. J Am Chem Soc 1994;116:9763-9764.
53. Qu X, Komatsu T, Sato T, Glatter O, Horinouchi H, Kobayashi K, Tsuchida E. Structure, photophysical property, and cytotoxicity of human serum albumin complexed with tris (dicarboxymethylene)[60]fullerene. Bioconjugate Chem 2008;19:1556-1560.
54. Wilkinson F, Helman WP, Rossa AB. Quantum yields for the photosensitized formation of the lowest electronically excited singlet-state of molecular-oxygen in solution, J Phys Chem Ref Data 1993;22:113-262.
55. Lu G, Komatsu T, Tsuchida E. Artificial hemoprotein nanotubes. Chem Commun 2007;2980-2982.
56. Lu G, Tsuchida E, Komatsu T. Human serum albumin nanotubes comprising layer-by-layer assembly with polycation. Chem Lett 2008;37:972-973.
57. Qu X, Lu G, Tsuchida E, Komatsu T. Protein nanotubes comprised of an alternate layer-by-layer assembly using a polycation as an electrostatic glue. Chem Eur J 2008;14:10303-10308.

Microvascular Reviews and Communications

Vol.3 No.1

Exogenous nitric oxide increases microflow but decreases RBC attendance in single capillaries in rat cerebral cortex

Minoru Tomita[1)], Takashi Osada[1)], Miyuki Unekawa[1)], Yutaka Tomita[1)], Haruki Toriumi[1)] and Norihiro Suzuki[1),*]

1) Department of Neurology, School of Medicine, Keio University

Abstract

The effects of nitric oxide (NO) on microflow and capillary red blood cell (RBC) velocity of the cerebral cortex were examined in 5 urethane-anesthetized rats through an open cranial window. Changes in microflow were evaluated with hemodilution technique with in-house Matlab-domain software, KEIO-IS1, presented as a 2-D microflow-map. When FITC-labeled RBCs were injected into the femoral vein, they appeared in the microvasculature of the cerebral cortex including capillaries. Changes in RBC velocity and attendance in single capillaries were determined with a high-speed camera laser scanning confocal fluorescence microscope before, during and after NO administration. The velocity and number of RBCs in the ROI were calculated with KEIO-IS2. Nitroprusside (a NO donor) was administered topically on the exposed brain surface, additionally microinjected into the tissues in 3 rats, and further intravenously in 2 rats. We found that: 1) NO increased microflow markedly regardless of the routes of administration and when limited to the cases of topical application microflow increased by 182±22 % (mean ± SD) of control ($P<0.01$). 2) RBC velocity in capillaries remained broadly unchanged, whereas RBC number (attendance) decreased in all cases ($P<0.05$). We interpreted that NO induced an increase in microflow not through nutritional capillaries but via other pathways from artery to veins, *e.g.*, thoroughfare channels. This finding suggests the presence of an independent velocity-impedance mechanism at the level of individual single capillaries in which excessive increase in capillary flow is somehow prevented. [MVRC 3(1): 11-16, 2009]

Key words: capillary flow, flow regulation, neuro-capillary coupling, RBC velocity, single capillary, tissue perfusion

Received 2009/4/4, Accepted 2009/8/4

*To whom correspondence should be addressed: Norihiro Suzuki, MD. PhD. Department of Neurology. School of Medicine, Keio University 35 Shinanomachi, Shinjuku-ku, Tokyo 160-8582, Japan
TEL: 81-3-3353-1211 FAX: 81-3-3353-1272
E-mail: nrsuzuki@sc.itc.keio.ac.jp

Introduction

Arterioles have been implicated in the control of capillary flow, feeding nutrition to neurons which dispatch time-to-time feedback signals to the arterioles concerning their nutritional requirements arising from their functional activities. However, recent studies have revealed that sudden neuronal activation causes capillary flow changes on a time scale of less than 1 s[1]. This time seems to be too short for the response to be controlled by arterial blood supply, suggesting the existence of a direct flow control mechanism operating from neurons to nearby capillaries. We showed RBC capillary flow decrease when cortical spreading depression and therefore neuronal depolarization was induced by potassium application on the brain surface of rats[2]. Involvement of intrinsic nitric oxide (NO) as a chemical mediator from neurons to capillary was postulated by Hudetz[3]. In fact, it is a gaseous material, which would afford a very rapid response in vascular dilatation[4] or tonic regulation[5]. However, capillary does not have muscles in possession. NO has a dual effect on cerebral tissue: NO is a poison that rapidly intoxicates neurons[6,7], while it increases cerebral blood flow greatly. It is still unclear whether or not exogenous NO is beneficial to neurons under ischemic conditions.

The aim of this study is to investigate the effects of exogenous nitric oxide (NO) on RBC velocity changes in cortical single capillaries following application of NO via various routes.

Methods and Materials

Five Wistar male rats were used. The experiments were approved by the Animal Ethics Committee of Keio University, and experimental procedures were performed in accordance with the University guidelines for the care and use of laboratory animals. The effects of nitric oxide (NO) on microflow whose definition will be given below and red blood cell (RBC) velocity in single capillaries were examined in urethane-anesthetized rats through an open cranial window. A femoral artery and a femoral vein were catheterized to measure blood pressure (SABP) and to allow administration of FITC-labeled RBC suspension prepared beforehand, respectively. A catheter was also inserted into the internal carotid artery for the injection of a small amount of saline (we used the saline as a negative indicator of blood in the present study). The external carotid artery was tied to avoid indicator escaping to the external carotid system. The animals were placed on a head holder with ear bars. A 5-mm-diameter cranial window was trephined above the left temporoparietal cortex and the dura was removed. The microvasculature in the cortical tissue was continuously videotaped with a conventional 30 fps (frames per second) video camera (Fig. 1). A FITC-labeled RBC suspension was injected into the femoral vein so that the labeled RBCs were circulating at the concentration of 0.4% of the total RBCs for approximately 3 hours after the injection.

Microflow: The principle and assumptions underlying the measurements of flow in 'pixels' (100 averaged Scion pixels or practical size 40 μm × 40 μm) were described elsewhere[8]. Briefly, when a dye was injected into the internal carotid artery, the dye was distributed to microvasculature to all corners of cerebral cortex: the bolus of blood passed through all pixels producing time-variable concentration

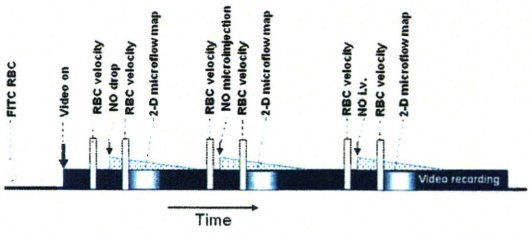

Fig. 1. Protocol of experimental procedure. Video recording of brain surface started at the closed arrow. NO was applied on the brain surface at NO drop. RBC velocity and number was measured with the high-speed camera laser scanning confocal fluorescence microscope during 10 s at the empty square. At the whitening marks in the dark bar, small amount of saline was injected into the internal carotid artery to produce hemodilution process which was recorded on the video tape and analyzed with KEIO-IS1 The dotted triangle area indicates NO effective period. NO was microinjected into the cortex and above set measurements were repeated. At NO i.v., NO was injected intravenously into the circulating blood. Above set measurements were repeated.

changes in the pixel as appearance, peaking and disappearance reflecting blood flow rapidity. The cortical images with dye dilution process were continuously recorded on videotape at 30 fps or directly fed into a personal computer through a Scion LG-3 frame grabber card (Scion Corporation, MD, USA). The dye dilution curves for all the individual pixels of an approximately more than 50 × 50 matrix (the size of the matrix was automatically decided by the computer in the ROI of ca. 4 mm × 5 mm) were all together analyzed with in-house Matlab-domain software, KEIO-IS1*1 to evaluate the MTTs by employing a customized algorithm of the area/height of hemodilution curves ($MTT = \int t.c(t)dt / \int c(t)dt$) where c is the optical density change in a pixel). The reciprocal mean transit time (1/MTT) was taken to represent the microflow (so termed by us), which was arranged in appropriate coordinates to construct a two-dimensional (2-D) microflow map with aid of KEIO-IS1. The 2-D flow map had a resolution of 625 flow values/mm^2, which is ca. 500-fold higher spatial resolution than that of conventional laser Doppler flowmetry. The KEIO-IS1 thus calculated automatically all pixular flow values in the region of interest (ROI) yielding a distribution curve of individual miroflows, and displayed a 2-D microflow map together with the histograms of microflow plotted against magnitude of flow rates. The unit of microflow was just relative or flow index relative to the control. However, time to time and location to location changes in flow value could be quantitatively compared.

---

*1 KEIO-IS1 (Patent No. 4068098) has potentially a wide applicability to analyze videotaped optical density changes of dye-dilution process in various organs, e.g., heart, liver, skin, stomach etc., to calculate reciprocal mean transit times of a dye, microflow mapping and analysis of microcirculatory parameters such as mean of flow values, standard deviation, skewness and kurtosis employing the moment analysis formula9). IS stands for initials of Istvan Schiszler, a Hungarian MD who stayed with us at age 26 (1998-2001) as a JSPS researcher. KEIO-IS2 (Patent No 4068099) has also been developed by him with a wide applicability to trace or track movements of fluorescence labeled cells or molecules. Those who are interested in the softwares running on PC. please contact Yutaka Tomita <yutakacnrs@aol.com>.

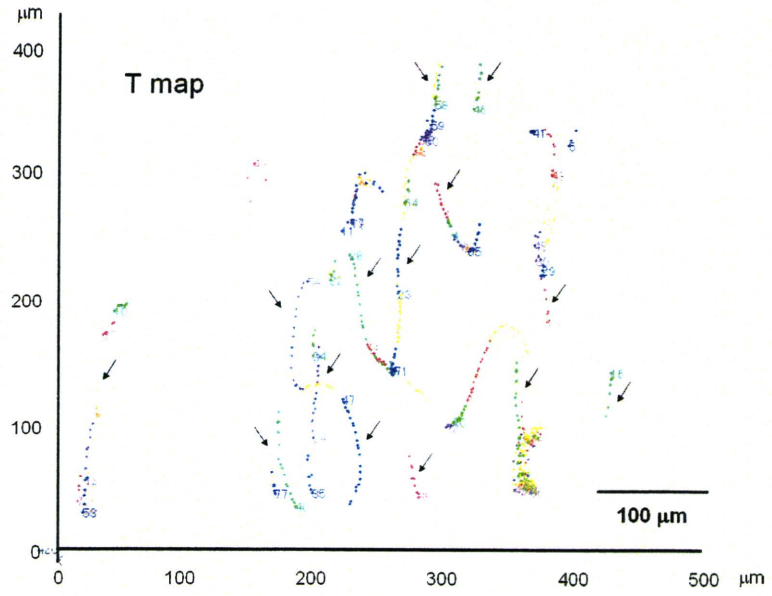

Fig. 2. RBC tracking map (T map) obtained with KEIO-IS2 from a 2 s video clip taken at 500 fps. Frame-by-frame movements of all RBCs appearing in the sequential 1000 frames are all shown. RBCs were automatically numbered in order of appearance. Arrows indicate RBC tracking in single capillaries.

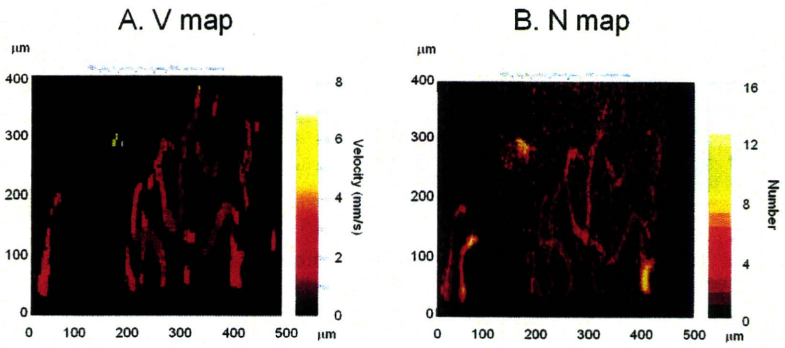

Fig. 3. A. RBC velocity map (V map) and B. RBC number map (N map), calculated with KEIO-IS2 from the same video clip as used for Figure 2. Color scales are shown at the right of the each figure. The RBC velocities in V map were calculated from moved distances per frame multiplying by the frame rate (500 fps). N map represents all RBCs that appeared in the ROI during 2 s, or integration of all 1000 frames. Note that the V map and N map resemble each other although their image elements were different.

Capillary RBC velocity: RBC velocity in single capillaries was examined with microscope in a central small area of 400 μm × 500 μm in the same cortical area as used for the above microflow measurement (the area was approximately 1/100th of a 2-D microflow map). The measurement was done by switching the optical system to a high-speed camera laser scanning confocal fluorescence microscope. A tracer FITC-labeled RBC which had been injected previously into the femoral vein was seen in arteries, capillaries and veins in the cortical microvasculature. The vast number of RBCs were analyzed with in-house Matlab-domain software, KEIO-IS2[10,11]. The software KEIO-IS2 automatically calculated velocities of all RBCs and displayed an RBC tracking map (T map, Fig. 2), an RBC velocity map (V map, Fig. 3: left), and an RBC number map (N map, Fig. 3: right). The numerical data of individual RBC velocities in single capillaries were further exported to a Microsoft Excel spreadsheet for statistical analyses[12]. On the tracking map, we sorted RBCs flowing in single capillaries (Fig. 2) and their velocities and numbers were exported to a spreadsheet Excel for further statistical analysis.

NO administration: A small amount of nitroprusside (3-5 mg/ml), a donor of NO, was topically applied in all cases on the brain surface. Additional application was made intraparenchymally with a microinjector in 3 cases, and intravenously from the femoral vein (i.v.) in 2 cases. The experimental protocols were schematically summarized in Figure 1. FITC-labeled RBC was injected into the femoral vein (at the empty arrow). Video recording made throughout the experiments starting at the closed arrow. NO was applied on the brain surface at mark A. Recording with high-speed camera laser scanning confocal fluorescence microscope during 10 s was interspaced at empty squares to monitor RBC movements for the calculation of RBC velocity and